IEEE Access
Multidisciplinary | Rapid Review | Open Access Journal

Received 5 August 2022, accepted 16 August 2022, date of publication 22 August 2022, date of current version 29 August 2022.

Digital Object Identifier 10.1109/ACCESS.2022.3200681

SURVEY

A Comprehensive Review of Grid-Connected PV Systems Based on Impedance Source Inverter

IHAB JAMAL[1], MAHMOUD F. ELMORSHEDY[1,2], (Member, IEEE), SHERIF M. DABOUR[1], (Senior Member, IEEE), ESSAM M. RASHAD[1], (Senior Member, IEEE), WEI XU[3], (Senior Member, IEEE), AND DHAFER J. ALMAKHLES[2], (Senior Member, IEEE)

[1]Electrical Power and Machines Engineering Department, Faculty of Engineering, Tanta University, Tanta 31521, Egypt
[2]Renewable Energy Laboratory, College of Engineering, Prince Sultan University, Riyadh 11586, Saudi Arabia
[3]School of Electrical and Electronic Engineering, Huazhong University of Science and Technology, Wuhan 430074, China

Corresponding author: Mahmoud F. Elmorshedy (mahmoud.elmorshedy@f-eng.tanta.edu.eg)

This work was supported by the Prince Sultan University.

ABSTRACT The increase in linking photovoltaic (PV) power plants to utility grids are due to the world expansion in PV systems and its advantages of low running cost, renewable, etc. Although PV is now considered one of the main power sources in many countries, it has low efficiency. Therefore, the big issue to improve the efficiency is to enhance the interface inverters' efficiency. Different inverter topologies have been proposed to relate to the PV panels; each has advantages and disadvantages. These topologies can be classified into two-stage and single-stage (impedance network) inverters. Impedance network inverters overcome the problems of traditional inverters and seek to realize the advantages of a two-stage system and reduce the number of power conversions. However, to the authors' best knowledge, there is no comprehensive review of the applications of the impedance source inverter for the PV system, including the control techniques. Therefore, this paper reviewed the existing topologies by paying attention to four key research issues: 1) various impedance network inverters and discusses the main structures from the point of view of the PV application, 2) control techniques suitable for impedance source inverters, comparing them in terms of complexity and theoretical performance, 3) investigation into the most important control methods used to connect the inverter output current with the network voltage, and 4) Challenges and future direction. Finally, this paper is provided as a brief reference to help researchers choose the appropriate impedance source inverter topologies for their applications and the preferred control and modulation methods for this type.

INDEX TERMS DC-AC power converters, pulse width modulation (PWM) converters, voltage-source converters, inverters, phase control.

I. INTRODUCTION

In the issue of climate change and environmental pollution is one of the issues of international attention. Therefore, the increase in investment shares in clean energy sources has become a strategic target globally. PV energy systems are the most used in both stand-alone and grid connected.

A. BACKGROUND AND CONTEXT

Research in the PV systems aims to raise the efficiency and quality of cells, operate the PV arrays to produce their maximum power, reduce the size and number of components in the system to limit cost and power losses, and raise the efficiency of the inverter used in power conversion, which is the most important component of the system. The impedance network inverters can be considered a promising means of converting power between the source and load in various electrical power conversion applications. Many structures of the impedance networks are provided with different control methods to use them in various applications, such as adjustable speed engines, uninterrupted power sources (UPS), distributed generation, and Electric vehicles [1].

B. LITERATURE SURVEY

Since the first appearance of Z-source inverter (ZSI) in 2006, many forms of modified and new impedance networks have

The associate editor coordinating the review of this manuscript and approving it for publication was Inam Nutkani.

been developed with (Buck and Boost) capabilities [1], [2], [3], [4], [5], [6], [7], [8], [9], [10], [11], [12], [13], [14], [15], [16], [17], [18]. This field is very wide and opens new doors in power electronics for different applications. One objective of this paper is to discuss the different topologies and then give much focus on ZSI and studies its development since 2002. Recently, modifications of ZSI and its new structures have increased dramatically with the increase in publications. Over the past two decades, nearly 2,000 papers and a summary of Z-source impedance structures are shown in Fig. 1.

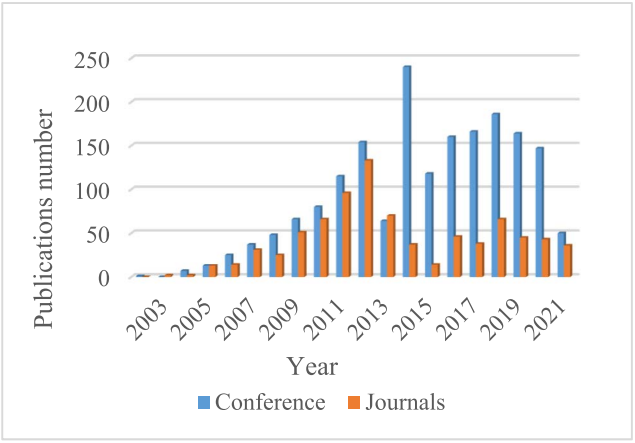

FIGURE 1. Numbers of publications (total 2135 as of Oct. 2021).

C. RESEARCH MOTIVATIONS

PV applications are classified into stand-alone or grid-connected PV systems (GCPVSs), where a central grid system is designed to increase the capacity of the main grid. Further, the number of power conversion stages for both stand-alone and GCPVSs can be categorized into single-stage and two-stage inverters. These classifications rely on the voltage source inverter (VSI) or current source inverter (CSI) as a major component. However, VSI has some drawbacks, first, the DC input voltage must be greater than the AC output voltage ($v_{ac} = \frac{V_{pv}}{2}$). Second, the upper and lower switches of the bridge cannot be operated in one phase leg simultaneously. This may cause a short circuit to the switches and destroy the inverter [5]. Hence, a time interval (dead time) must be used between the switching pulses of the upper and lower devices, which results in a distortion of the inverter's output waveform. Therefore, there are two ways to overcome the problem of the DC-link voltage value. Firstly, a line frequency transformer can be added on the AC side to raise and modify the value of the AC voltage to match the grid voltage. Secondly, a DC voltage boost converter can be added before the inverter. To achieve the required DC voltage, resulting in complicating the entire system, reducing efficiency, and increasing cost [2]. However, the use of dead time is still necessary if any of the above two methods are used. Therefore, ZSI is proposed to eliminate these obstructions, using the shoot-through (ST) states to achieve boosted DC-link voltage. Dead time can also be avoided since the ST state will become part of the inverter's operating states and the active and null states of conventional VSI. However, the traditional ZSI has some drawbacks, such as [1]:

- In the case of ZSI, the DC-link voltage is less than the Z-source capacitor's voltage, which increases capacitor size.
- Small boosting capability.
- The ZSI input current is not continuous due to the diode's effect, which may be undesirable for PV.
- The inrush current in ZSI at start-up is very high.

To overcome the drawbacks of the original ZSI, much research has been done, and a set of modified ZSI topologies have been proposed [12], [15]. These proposals aim to raise the efficiency of ZSI by increasing capacitance, decreasing component stresses, and decreasing the number of switches, switching frequency and passive components [20]. Moreover, different structures have been suggested to increase the reinforcement capacity but did not solve other problems of traditional ZSI [21]. Further, in [39], [43], [44], [45], [46], and [47], other topologies have been proposed to reduce the voltage of the Z-source capacitor, but they cannot fully increase the boosting capacity of the inverter. Generally, every structure has its successes and failures in solving various defects, so the optimal topology cannot be determined easily.

D. RESEARCH AIMS

As mentioned earlier, many ZSI topologies have been developed and tweaked where each topology has its unique features and applications that suit it best, and there is no one-size-fits-all solution. It is expected that new ZSI topologies will be constantly rolled out to meet and improve the performance of the inverter for different applications. Among them is the generation of renewable energy, such as PV, due to the unique ability of the ZSI to boost voltage with a minimal number of components and potentially low cost. Nevertheless, different modulation strategies are also needed to operate the inverter switches and adjust them to get the required outputs like frequency, the amplitude of voltage, and current. Different PWM schemes can control impedance source inverters with the same input and output relations, such as sinusoidal PWMs (SPWM) [83], [84], [85] and space vector PWM (SVPWM) [87], [88], [89], [90], [91], [92], [93], [94], [95], [96], to control the output voltage. There are limited numbers of review papers focusing on specific targets, for example, the work in [3] studying and developing the modification schemes suitable to this family of power inverters only. Also, other reviews have been concerned with studying different structures, advantages, and drawbacks [1], [3], [18], [42], [43], [44], [56]. Further, some reviews focused on studying reaction energy only [55]. Meanwhile, few reviews tried to study and cover different topologies, PWM techniques, and control strategies [5], [12], [57]. In [12] there are two-part studies. The first part was concerned with all the topologies. The second part gave a brief study of the control strategies on

the DC side, and another brief for the most important methods of PWM techniques. While they neglected the necessary control strategies on the AC grid side. Finally, [5] is a good review article, but it was a little old. It did not mention new types of impedance networks such as (Y-source, T-source, SL-ZSI, and SBI) and it did not cover the technique of 3rdHI-CB-PWM. This paper presents a complete review of the most important studies and literature specializing in the parts of the grid-connected PV systems based on impedance source networks (ISNs) inverters. The second section of this paper is concerned with classifying the impedance source networks-based inverters, describing their different structures, and then comparing them in terms of characteristics, number of components and drawbacks. In the third section, the paper categorizes the different modulation techniques with detailed explanations and qualitative comparisons. In the fourth section, what has been published in the literature from the different control strategies that have been previously applied are reviewed. Thus, it is within the researcher's reach to choose the appropriate impedance source network topology for the target application and how to operate the inverter switches by controlling the pulse width. Finally, determining the control strategy that achieves the best performance for each system stage.

II. IMPEDANCE NETWORK CLASSIFICATIONS

The Z-source inverter (ZSI) was first introduced thirty years ago with a unique circuit where it can boost the input voltage. It has been used as a single-stage inverter in different applications, such as in the conversion systems of renewable energy sources. Using the Z-source impedance network (ZSN) features, the inverter can be controlled in both Shoot-through (ST) and Non-Shoot-Through (NST) states, as will be explained later in the following section. Although the ZSI can simultaneously perform the booting and inversion operations, it suffers from drawbacks, such as a discontinuous input current. This drawback is solved by deriving another topology called the quasi-Z-source network (QZSN), introduced in 2008 [5]. This circuit is characterized by continuous DC input current. After that, many impedance circuits are developed by bypassing a specific defect in the original network to improve the inverter properties [7]. Therefore, the main aim of this paper is to review the Impedance Source Networks (ISNs) coupled with VSI and clarify the advantages and disadvantages of each type [8].

The ISNs can be classified based on magnetic and transformer coupling into non-transformer-based and transformer-based types, as shown in Fig. 2. It can also be divided into the following groups [9]:

a) ISNs including inductive components,
b) ISNs including magnetically coupled inductive components,
c) ISNs including a transformer, and
d) ISNs including an active switch.

One advantage of ISN that includes magnetically coupled transformers is that they may have a high voltage boost factor

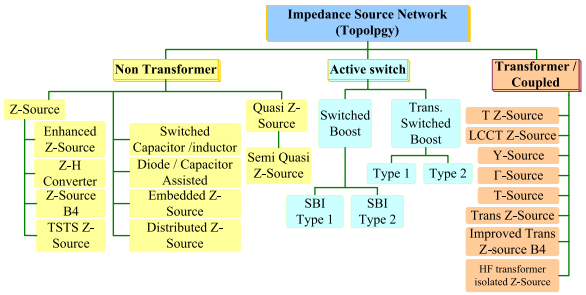

FIGURE 2. Classifications of the different ISNs topologies [9].

TABLE 1. Impedance source networks classification [5].

Input current	Non-transformer	transformer-based	Active switch
Discontinuous	▪ ZSI ▪ Switched capacitor /inductor	▪ Trans-ZSI ▪ Y-source ▪ T-ZSI ▪ LCCT-ZSI ▪ Γ-ZS ▪ T-source	▪ SBI Type1 ▪ SBI Type 2 ▪ The SL-SBI type 1
Continuous	▪ Quasi-ZSI ▪ Diode/capacitor assisted ▪ E-ZSI	▪ E-ZSI ▪ Trans-QZSI ▪ Trans-QZSI + CCM ▪ LCCT-QZSI	▪ Trans. SBI Type1 ▪ Trans. SBI Type 2. ▪ SL-SBI type 2.

according to turn ratio. Table 1 divides ISNs into two categories according to the type of input current; discontinuous input current (DIC) and continuous input current (CIC) [10]. In general, the impedance source inverter operates in two modes of operation as follows:

- Same as VSI when the input voltage is higher or equal to the required voltage level (modulation index is $M \leq 1$).
- Like a step-up transformer, when the input voltage level is lower than the required voltage level; thus, the VSI operates in ST mode to boost the input voltage level.

The ZSN is the original impedance network from which all other ISNs topologies were derived, either by modifying or rearranging the locations of inductors and capacitors [5], [6], [7], [8], [9], [10], [11], [12], [13], [14], [15], [16], [17], [18], [19], [20]. Each ISN topology has specific features to meet the needs of a particular application. The new ISN topologies are being developed so far for the following reasons:

- Reducing the quantity and rating of ISN components,
- Increasing the voltage gain factor,
- Realizing higher power density, and,
- Increasing the inverter efficiency.

Components such as inductances, capacitors, auxiliary diodes, or switches can be rearranged or increased to increase the network voltage. Fig. 3. shows the required components for each topology. Each topology has its advantages and disadvantages, as will be briefly discussed in the following subsections.

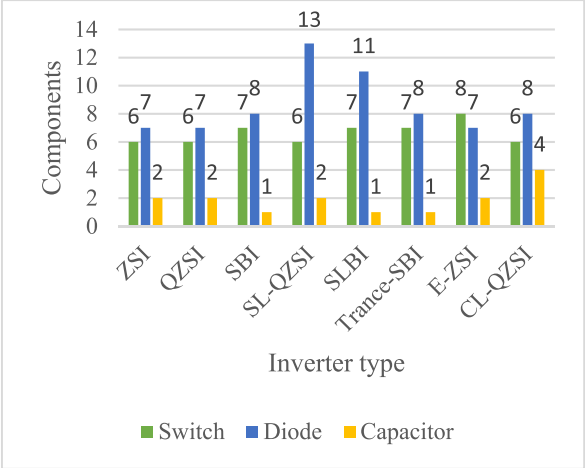

FIGURE 3. Required components for ISNs topologies.

A. NON-TRANSFORMER BASED CONFIGURATIONS

These ISNs do not contain a transformer where they consist of only passive components. More details about these configurations are provided in the following sections.

1) Z-SOURCE AND Quasi-Z-SOURCE

As mentioned earlier, ZSI topology has appeared as an alternative to the traditional VSI or CSI. The ISN is considered a buffer between the source and the inverter bridge. It provides short circuits or open circuits at any time to suit the operating mode. Conventional ZSN, shown in Fig. 4(a), suffers from several problems, including that it draws discontinuous input current from the source, and it is not suitable for very low input DC voltages. Therefore, different voltage topologies derived from the ZSI have been proposed, such as QZSI. Two types of QZSI are shown in Fig. 4(b) and (c), where it is used to improve the performance of ZSI and overcome its drawbacks [5], [6]. where V_{in} equals the input DC voltage or PV voltage, V_{dc} the boost voltage produced by the Z-source impedance, V_C the voltage across the Z-source capacitor, Do the duty ratio of the shoot-through interval, and B the boost factor of the impedance network.

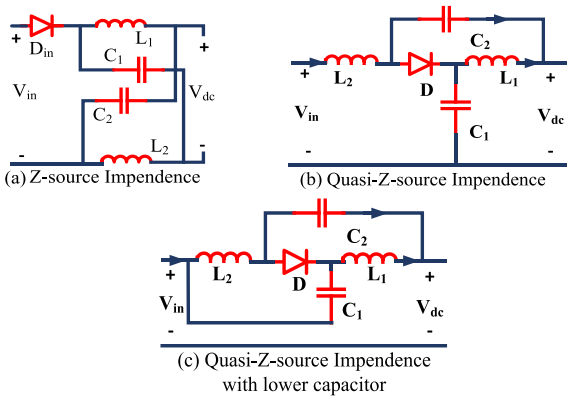

FIGURE 4. ZSI topologies [5], [6].

2) EMBEDDED-Z-SOURCE NETWORK (E-ZSN) [6]

An E-ZSN provides a continuous input current to the inverter, has a low capacitor voltage and is particularly suitable for PV applications [12]. Figure 5(a) shows the topology of the E-ZSN circuit. This structure reduces the voltage and current ripple by using two independent DC voltage sources. But it increases the number of components and their cost. For this reason, E-ZSN is preferred in the case of PV arrays or fuel cells. The disadvantage of E-ZSN is that it operates asymmetrically at asymmetric input voltage. In the E-ZSN, inductors L_1 and L_2 are considered input current filters rather than external LC filters.

3) SWITCHED INDUCTOR/CAPACITOR

Following One of the most common methods is using a switched inductor instead of a permanent inductor which improves the boost ratio of the inverter, reduces the stress on the passive components and eliminates the star-up inrush current [39], [43], [44]. The switched inductor ZSI is shown in Fig. 5(b). The switched inductor ZSI and QZSI provide a continuous input current and low voltage stress on the capacitor. The embedded ZSN with a switching inductor combines the advantages of both switched inductors ZSI (SL-ZSI) and (E-ZSI). Such as high boost ratio, low capacitor voltage stress, and low input current ripple. However, the switched inductor topology needs many passive devices, which increases the inverter cost. A switched capacitor can also be used instead of a permanent capacitor to achieve the same advantages.

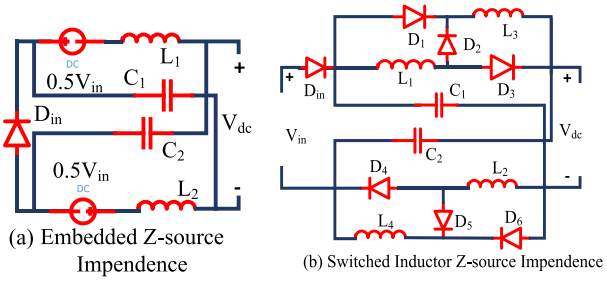

FIGURE 5. Advanced ZSI topologies.

4) CAPACITOR/DIODE ASSISTED [14], [15]

Some capacitors and diodes are added to the QZSI circuit to increase the voltage boost capability in this topology. Fig. 6(a) shows the Diode Assist Extended Boost (DAEB), in which one capacitor (C_3), one inductor (L3) and two diodes (D2 and D_3) are added to a conventional QZSI. Fig. 6(b) shows the modified diode assisted (MDAEB), which is derived from DAEB-QZSI by changing the contact points of the capacitor C_3. Theoretically, such modifications can produce unlimited boosting capability, but this is impossible due to power losses. This structure is characterized by the capacitor's high voltage gain and low voltage stress. However, the passive components are increased. Therefore, Capacitor Assist Extended Boost (CAEB) topology, shown in Fig. 6(c), is preferred because

it requires fewer semiconductor devices and has less power loss.

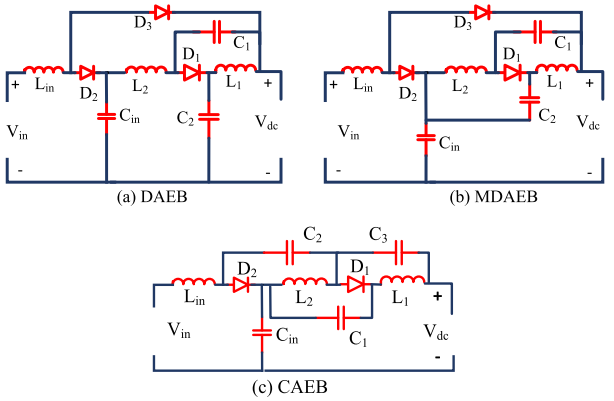

FIGURE 6. Capacitor/diode assisted topologies.

B. TRANSFORMER BASED OR MAGNETIC COUPLING CONFIGURATIONS [1], [2]

A general method was proposed to clarify the derivation of magnetically coupled networks in [1] and [2]. It was found that magnetically coupled inductors and transformers improve the voltage boosting ratio and modulation index of the ISNs. It also decreases the passive components used in the network, increases the quality of power density, and reduces the system's cost. The following sections describe the ISNs topology based on the transformer or the coupled inductor.

1) TRANS-Z-SOURCE, TRANS-QZ-SOURCE, TRANS-QZ-SOURCE WITH CCM [8], [17], [20]

Theoretically, the original ZSN, QZSN and embedded-ZSN have unlimited voltage gain. However, if a voltage gains higher than 2 or 3 will result in a higher stress voltage on the switches. Trans–ZSN has been proposed with a discontinuous input current [13]. Trans-QZSN, and Trans-QZSN with continuous conduction mode (CCM) have been proposed [14]. These proposals aimed to obtain higher voltage gains while keeping lower voltage stress and reducing the ZSN components to one coupled inductor, one capacitor, and one diode in Trans-QZSN.

Meanwhile, an additional capacitor is added to the Trans-QZSN-CCM. In Trans-ZSN, the boost factor is increased, and the coupled inductors are used as energy storage. The disadvantage of this topology is the presence of leakage inductance. Fig. 7., shows the Trans-ZSN, Trans-QZSN, and Trans-QZSN with CCM.

2) Y-SOURCE NETWORK [48]

The Y-source network belongs to the networks with magnetically coupled components and consists of an inductor coupled with three coupled windings (N_1, N_2, and N_3), as shown in Fig. 8(a). Theoretically, the proposed inverter can obtain any voltage gain by adjusting the turns ratio and ST duty cycle of the switch. The disadvantage of this scheme is the presence of leakage inductance. The disadvantage of this scheme is the presence of leakage inductance.

3) THE Γ - Z-SOURCE NETWORK [10]

In Fig. 8(b), the Γ-ZSI consists of one capacitor and a two-windings coupled transformer in the ISN to simultaneously increase the gain voltage and modulation index while decreasing the number of components. The Ã-ZSN has a discontinuous input current. The gain of the Γ-ZSN increases with decreasing turns ratio compared to the T-SN, trans-ZSN, or LCCT-ZSN, whose gain increases with the 'turns ratio [16] The disadvantage of this topology is the presence of leakage inductance, which may affect the voltage and current on the semiconductor.

4) THE T-Z-SOURCE NETWORK [4], [15]

The TZ-source achieves high voltage gain by setting the turns ratio of the transformer to greater than 1. The T-Z-source network contains magnetic components, which are a two-winding coupled inductor and one capacitor [17], as shown in Fig. 8(c). The voltage gain and boost factor of T-ZSI are higher than ZSI and QZSI. However, it has several drawbacks, including resonant effects. Because of that, transient currents can be high. Secondly, the substantial number of elements that make up this network and the fact that the input current is discontinuous.

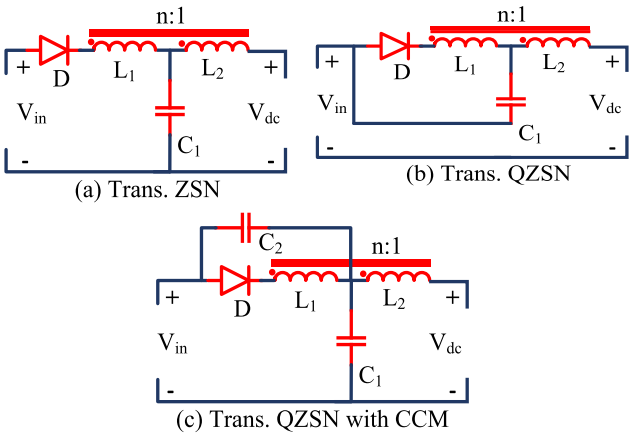

FIGURE 7. Trans. ISNs.

5) THE LCCT-Z-SOURCE NETWORK AND LCCT-QZ-SOURCE NETWORK [9], [3]

The LCCT-Z-source is derived from Trans-Z-source. It consists of an inductor-capacitor–capacitor-transformer Z-source network, as shown in Fig. 9(a), while the LCCT-QZSI is shown in Fig. 9(b). The transformer used in these networks is ideal and of high frequency. The LCCT circuit prohibits saturation from occurring in the transformer core. For energy storage during the boosting process, only one inductor is used. With the combination of the inductor and the transformer in

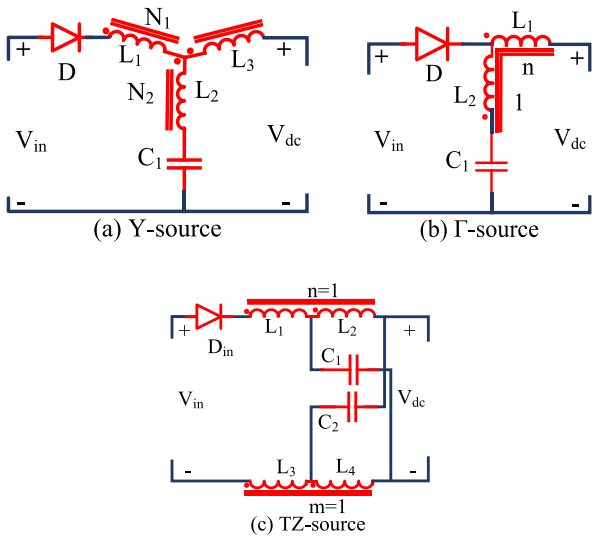

FIGURE 8. Advanced trans. ISNs.

a common core, the LCCT-ZSN realizes high voltage gain and a higher modulation index but has a discontinuous input current.

Meanwhile, the LCCT-QZSN collects high gain voltage and continuous input current at any load level. It also prevents high-frequency fluctuations from the input current. The LCCT circuit can be improved by using high switching frequency diodes.

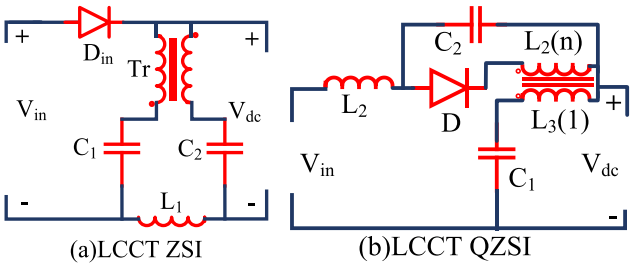

FIGURE 9. LCCT-Z-source.

C. SWITCHED-BOOSTED INVERTER (SBI) TOPOLOGIES

The switched-boosted inverter (SBI) was introduced as an alternative to ZSI with the advantage of half number of the passive components. The inverse Watkins-Johnson topology, which is suitable for low power applications, is derived from the SBI topology, as shown in Fig. 10. The impedance network consists of one inductor, two diodes, one capacitor and an active switch where the capacitor connects to the negative terminal of the DC source, and the diode connects to the positive terminal. This type is illustrated in Fig. 10(a) and named SBI Type 1. The arrangement of the passive elements is changed to present a new type called SBI Type 2, where the diode connects between the capacitor and the positive side of the DC source, as clarified in Fig. 10(b). It is noticeable that SBI and ZSI in the ST state are similar in operation. Also, SBI could not overcome the most of ZSI drawbacks, such as the high voltage stress on the capacitor, the low boost capacitance, and discontinuous input current [26].

1) TRANS-SBI TOPOLOGIES

In the Trans-SBI type, the number of inductors is increased into two in series inductors instead of one as in the original SBI. In Trans-SBI Type1, the capacitor is connected between the boost circuit and the positive terminal of the inverter input. Meanwhile, in Trans-SBI Type 2, the capacitor is connected between the boost circuit and the negative terminal of the inverter input. Fig. 10(c) and Fig. 10(d) show these two topologies [27].

2) SWITCHED INDUCTOR SBI TOPOLOGIES

The switched inductor boost inverter (SL-SBI) is offered for is offered for achieving higher DC-link voltage. It is an upgraded model from SBI, but the inductor has been replaced by a circuit consisting of two inductors, three diodes and a DC source. Several substructures are derived from the underlying SL-SBI to bypass some defects by modifying the location of the DC sources. When the DC voltage source is placed in the place of the DC_4, a constant and continuous input current can be obtained, and it is known as the SL-SBI Type-1. Whereas if the DC voltage source is placed in the position of the DC_2, the input current will be discontinuous, and it is called the SL-SBI Type-2 because the diode is connected in series with the DC source. Further, placing the DC voltage source in the position of DC_3 leads to an input current ripple. Both structures are shown in Fig. 10(e) and Fig. 10(f). [28].

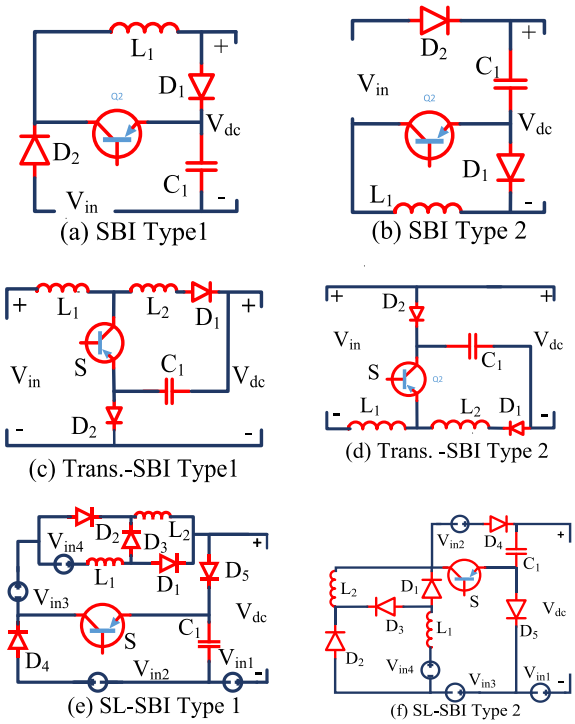

FIGURE 10. Switched boost inverter (SBI).

TABLE 2. Comparison of the configuration of ISNs.

Name	D	C	L	Integrated winding	Continuous I_{in}	Inrush I_{in}	Common Earthing
ZSI	1	2	2	-	No	Yes	No
QZSI	1	2	2	-	Yes	No	Yes
E-ZSI	1	2	2	-	Yes	Yes	Yes
Trans-ZSI	1	1	-	2	No	Yes	Yes
Trans-QZSI	1	1	-	2	Yes	No	Yes
LCCT-ZSI	1	2	1	2 windings coupled inductor	No	No	Yes
LCCT-QZSI	1	2	1		Yes	No	Yes
Γ- ZSI	1	1	1		No	Yes	Yes
T-ZSI	1	2	-	2 integrate 2 windings	No	Yes	No
Y-SI	1	1	-	Integrate 3windings	No	Yes	Yes
SL-ZSI	7	2	4	-	Yes	Yes	No
CEAB	2	3	3	-	Yes	No	Yes
DEAB	3	4	3	-	Yes	No	Yes
SBI	2	1	1	-	No	Yes	No

where D is the diode, L the impedance source network inductor, and C the impedance source network capacitor. From the table it can be concluded that the topologies derived from the ZSI construct draws a discontinuous input current and has a high inrush current. In contrast to the topology derived from QZSI.

D. SUMMARY

Several modifications and improvements have been proposed in the original ZSI to overcome the drawbacks of the traditional ZSI and improve its performance [8], [9]. Some succeeded in increasing the boosting capability, and others reduced the capacitor voltage and the start-up inrush current. Thus, each ISNs derived from the ZSI has advantages and disadvantages in solving the problems of the original configuration, so the user may not be able to select the appropriate network in practice quickly and accurately. Hence, to help the researcher determine the appropriate type required to achieve the objectives of the application, Tables 2 and 3 summaries the differences between the most famous types of ISNs in terms of components and characteristics, respectively. In contrast, Table 4 compares ISNs topologies in terms of advantages and disadvantages.

III. MODULATION TECHNIQUES

Impedance source inverters represent a different generation of power conditioning systems called single-stage inverters because they simultaneously adopt boost capability and reversal process. Therefore, it is an alternative to two-stage systems [1], [2], [3], [4], [5], [6], [7], [8]. Thus, the research activities have increased to improve the performance of ZSI from different perspectives, such as voltage gain, voltage stresses across devices, input current continuity, and switching efficiency [5], [19], [20], [21], [22], [23], [24], [25]. Among these are the various topological improvements already mentioned in the second section. It is noteworthy that all these improvements did not affect the basic operating principle of the original ZSI, as shown in Fig. 11. This refers to using an additional switching case compared to the standard cases of operating a three-phase voltage source inverter (VSI). This additional state is called the shoot-through state (ST) and is responsible for boosting the input voltage.

During this condition, the bridge appears as a short circuit by turning on at least two switches of the phase leg at the same time, as shown in Fig. 11(a).

On the other hand, during the non-ST states, the bridge is equivalent to a current source (Because the inverter bridge operates in one of the six active states, therefore acts as a current source that is displayed from the ZSI network. Due to the symmetric in the circuit, both inductors have identical current value. During this mode, the DC voltage source appears across the inductor and capacitor. The capacitor is charged and power flows to the load through the inductor), as shown in Fig. 11(b). In contrast to the traditional VSI, which does not allow the presence of the ST state. Because of the use of an impedance network, this state is allowed in impedance network inverters and must be inserted into any of the zero states so as not to affect the active states and, thus, the output AC voltage. This is the function of the pulse width modulation controllers. Three-phase impedance source inverters can use any of the conventional modulation schemes discussed in [5], [19], [20], [21], [22], [23], and [34], or the SVM schemes presented in [5], [23], and [24] and hybrid modulation (HM) proposed in [34], but the ST case may not be taken advantage of without modifying these methods to fit the ZSI principle of operation.

In general, three-phase ZSI modulation schemes can be classified into two categories: carrier-based modulation

TABLE 3. Comparison of the characteristics of ISNs.

Name	Boost factor	V_{C1}	V_{C2}	V_{stress}
ZSI QZSI E-ZSI	$\frac{1}{1-2D_0}$	$\frac{1-D}{1-2D_0}$	$\frac{1-D}{1-2D_0}$	$\frac{V_{in}}{1-2D_0}$
Trans-ZSI	$\frac{1}{1-(n+1)D_0}$	$\frac{1-D}{1-(n+1)D_0}$	-	$\frac{nV_{in}}{1-(n+1)D_0}$
Trans-QZSI		$\frac{nD}{1-(n+1)D_0}$	-	
LCCT-ZSI	$\frac{1}{1-(n+1)D_0}$	$\frac{1-D}{1-(n+1)D_0}$	$\frac{nD}{1-(n+1)D_0}$	$\frac{nV_{in}}{1-(n+1)D_0}$
LCCT-QZSI				
Γ- ZSI	$\frac{1}{1-\left(\frac{n}{n-1}\right)D_0}$	$\frac{1-D}{1-\left(\frac{n}{n-1}\right)D_0}$	-	$\frac{V_{in}}{n(1-D_0)-1}$
T-ZSI	$\frac{1}{1-(2+n+m)D_0}$	$\frac{(1+n+m)D}{1-(2+n+m)D_0}$		$\frac{(1+n+m)V_{in}}{1-(2+n+m)D_0}$
Y-SI	$\frac{1}{1-(\frac{N_3+N_1}{N_3-N_2})D_0}$	$\frac{1-D}{1-(\frac{N_3+N_1}{N_3-N_2})D_0}$	-	$\frac{(1-\left(\frac{N_3+N_1}{N_3-N_2}\right))V_{in}}{1-\left(\frac{N_3+N_1}{N_3-N_2}\right)D_0}$
SL-ZSI	$\frac{1+D}{1-2D_0-D_0^2}$	$\frac{1-D}{1-2D_0-D_0^2}$	$\frac{2D}{1-2D_0-D_0^2}$	$\frac{(1+D_0)V_{in}}{1-3D_0}$
CAEB & DAEB	$\frac{1}{1-3D_0}$	$V_{C1}=\frac{1-2D}{1-3D_0}$ $V_{C3}=\frac{1-D}{1-3D_0}$	$V_{C2}=\frac{2D}{1-3D_0}$ $V_{C4}=\frac{D}{1-3D_0}$	$\frac{V_{in}}{1-2D_0}$

where V_{c1} and V_{c2} are the voltage of capacitors C_1 and C_2. V_{stress} is the voltage stress on the switches. In contrast to the basic impedance source network topologies, the transformer-based topologies and switched boost inverters have a high boosting ratio and high gain.

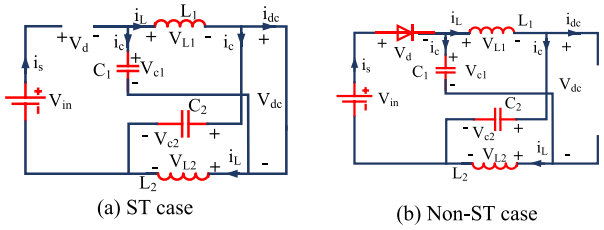

FIGURE 11. Modes of operation for ZSI.

schemes and space-vector-based modulation schemes. This section provides a comprehensive review with a comparative evaluation of these different modulation schemes to measure performance and show how each scheme's properties influence ZSI parameters, such as voltage stress across devices, voltage gain value, and maximum modulation index.

A. CLASSIFICATION OF THREE-PHASE ZSI MODULATION SCHEMES

Fig. 12. illustrates the various modulation schemes that are used with the three-phase ZSI, which can be classified into two categories according to the different ST states insertion methods.

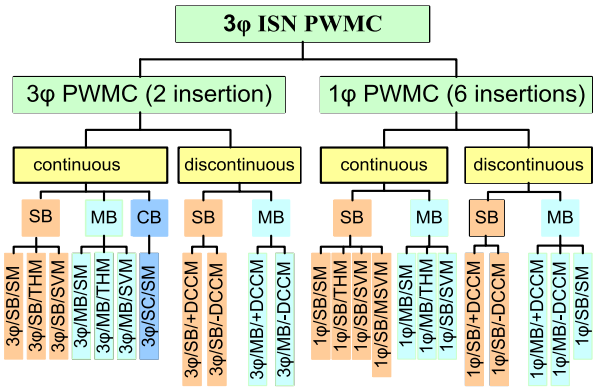

FIGURE 12. ZSI modulation schemes classification.

where SB is the simple-boost, MB is the maximum boost, CB is the constant boost, SM is the sinusoidal modulation, THM is the third-harmonic injected modulation, SVM is the space vector modulation, MSVM is the modified SVM,

TABLE 4. Comparison of the optimization results of different approaches.

Name	Advantages	Disadvantages
ZSI	• Bypassing VSI and CSI problems. • Operating both switches in the same phase and at the same time does not cause any damage. • Suitable for PV applications.	• Discontinuous input current. • High inrush current. • High capacitors voltage requires a large capacity. • ST duty ratio was less than 0.5.
QZSI	• Continuous input current. • Capacitors' ratings are decreased. • Current stress is lower than ZSI. • Suitable for PV applications.	• ST duty ratio was less than 0.5. • Not suitable for very low input DC voltage.
E-ZSI	• Draws smooth input current. • The input current and voltage ripples are less. • Suitable for PV applications.	• Uneven distribution of stress through the components due to the asymmetric structure. • ST's duty ratio was less than 0.5.
Trans-ZSI & Trans-QZSI	• The gain factor is higher than the ZSI and QZSI. • The stresses through components are reduced. • Suitable for PV applications.	• Discontinuous input current. • Transformers and coupled inductors increase volume and cost.
Y-Source	• It achieves a high gain factor by a small ST duty ratio. • It maintains a high boost factor and high modulation index. • Low THD in the output.	• Discontinuous input current. • Electromagnetic interference noise impact's reliability.
Γ- ZSI	• It achieves a high gain factor with a low turn ratio. • Has good spectral performance.	• Inductance leakage increases the voltage and current stress over devices.
LCCT- (ZSI, QZSI)	• High-frequency ripples are filtered in the source.	• High winding-turns ratio. • Electromagnetic interference noise impact's reliability.
CAEB & DAEB	• Theoretically, unlimited boosting capability. • High voltage gain • Low voltage stress on the capacitor.	• The passive components are increased. • High power losses.
Switched capacitor inverter	• Perform input operations without inductors. • A high switching frequency can be used to operate many stages of SCC cells. • Therefore, small size passive components (such as capacitors and inductors) can be employed. • The capacity to multiply voltage at high gain. • Capable of producing high multi-level voltage for high power applications when SCC cells are added in stages. • Modular construction that can be incorporated into many types of structures.	• Numerous components and large circuit size. • High power loss (switching losses) as a result of the necessity for a large number of power switches. • Significant transient currents (spike current)

From this table it can be summarized that the structures which includes a transformer or an active switch to the impedance source network structure have a high gain rate and a high boost ratio relative to the original structures such as ZSI and QZSI.

DCCM is the dc-clamped modulation, and HM is the hybrid modulation.,

More details about each category will be discussed as follows:

- Two ST insertion strategies: in which three-phase modulation schemes simultaneously operate through the three-phase legs as shown in Fig. 13(a). The ST states immediately replace the null states (111 and 000). This can be achieved using two straight DC lines, and the sinusoidal modulation signals of VSI. The ST duty cycle in this strategy is equally divided into two parts in one switching cycle. At each part, all three legs are in ST state, so that ST current is distributed evenly on three legs. On the other hand, the ST state inserts additional switch transitions. As a result, there are two more transitions in each leg than case of VSI in one switching cycle. [18]
- Six ST insertion strategy: in which single-phase modulation schemes operate through one phase at a time. The principle of this method is that the ST states are inserted at every transition by overlapping the upper and lower driver signals as shown in Fig. 13(b). The transmission intervals in one switching cycle are the same as in the VSI. The ST state is divided into six segments, so that equivalent switching frequency of the impedance network equals six times the switching frequency. So, the size of the inductors can be greatly reduced. [18]

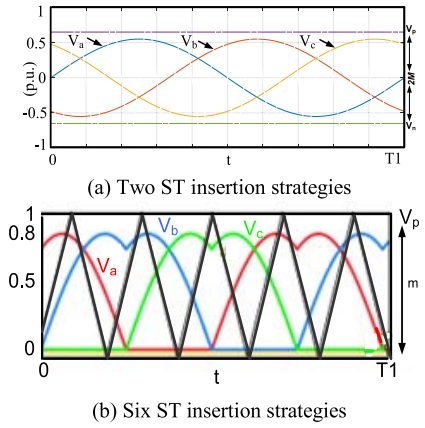

(a) Two ST insertion strategies

(b) Six ST insertion strategies

FIGURE 13. PWM types based on ST insertion.

Each of these two categories can be divided into two subcategories as follows: [29]

- Continuous modulation: Two additional reference voltages (V_p and V_n) are used with any of the reference signals (v_a, v_b, v_c) since the shape of V_p and V_n differs from one controller scheme to another.
- Discontinuous modulation: One additional reference voltage signal (V_p or V_n) is used with DCCM reference signals.

Any of the previous type also can be controlled using one of the following modulation techniques:

- Simple Boost control (SB),
- Maximum Boost control (MB),
- The Maximum constant boost pulse width modulation (MCBC),
- Constant Boost control with 3rd Harmonic Injection (THM),
- Modified Space Vector control (MSVPWM).

The literature discussed the use of the above methods in controlling pulse width modulation (PWM) in ZSI. In fact, each method is distinguished from others in several characteristics.

In case of using SBC or 3rd-HI-CBC, the ST ratio is controlled by MPPT. Thus, it is suitable for PV systems. As for maximum boost control (MBC), it is not suitable for PV systems because the variable ST ratio with MBC will not be able to track the reference envelope. Also, MBC requires increasing the size of the inductors and capacitors to remove low frequency ripples [30]. Therefore, the operating principle of each modulation method will be briefly explained. Moreover, a comparison of the most important differences is introduced in Tables 3.4 and 3.5.

1) SIMPLE BOOST CONTROL (SBC) [6]

This technique is the simplest PWM method to control the ZSI [20]. Two values V_p and V_n are used as ST modulation signals. As shown in Fig. 14., the positive and negative peak values of these signals are greater than or equal to the peak values of the three-phase sinusoidal reference signals. ST only occurs when the carrier signal is greater than V_p or less than V_n. Otherwise, it works like conventional sinusoidal pulse width modulation (SPWM). Fig.14 shows the simple boost pulse width modulation process and how to get the shoot-through interval.

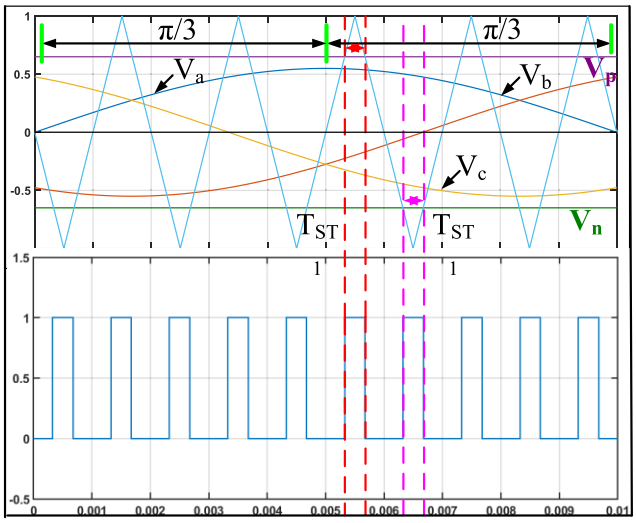

FIGURE 14. Description of the SBPWM.

2) MAXIMUM BOOST CONTROL (MBC) [25]

Fig. 15. shows the MBC technique. Compared with the SBC technique, MBC keeps the six active states of ZSI unchanged

and converts all zero (null) states to ST (zero) states. Thus, the maximum gain G value for any modulation index M is achieved without distorting the resulting signal. The ST modulation signals are not two fixed lines but the positive and negative envelopes of the three-phase reference signals. ST occurs when the carrier signal is greater than the positive envelope or less than the negative envelope. Since the duty cycle of ST differs in each cycle. So, the mean value of ST during the cycle is considered to calculate the gain.

The ST state is repeated periodically every $\pi/3$. Assuming that the carrier signal frequency is much higher than the modulation signal frequency, the equation for the ST during one switching period in the interval ($\pi/6$ and $\pi/2$) can be formulated as follows:

$$D_{\circ}(\theta) = \frac{2 - (Msin\theta - Msin\left(\theta - \frac{2\pi}{3}\right))}{2} \tag{1}$$

The average duty ratio of shoot-through can be formulated as follows:

$$D_{\circ} = \frac{1}{T}\int_{\frac{\pi}{6}}^{\frac{\pi}{2}} \frac{2 - (Msin\theta - Msin\left(\theta - \frac{2\pi}{3}\right))}{2} d_{\theta} \tag{2}$$

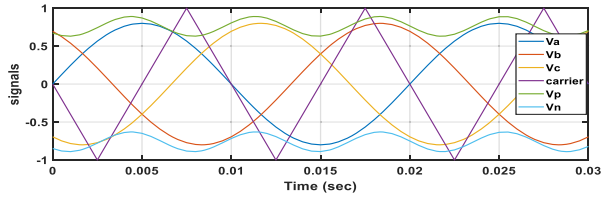

FIGURE 15. Description of the MBPWM.

But in the MB method, due to the periodic variation of the operating ratio D_o (t) per $\frac{\pi}{3}$, the inductor current has a current ripple equal to six times the load frequency, which raises the required inductance value.

3) MAXIMUM CONSTANT BOOST CONTROL (MCBC) [26]

Fig. 16. shows the MCB technique, which realizes the most voltage gain and keeps the ST duty ratio constant. Maintaining the ST constant reduces size and cost while increasing the voltage boost of any modulation index results in less voltage stress over the switches.

As in the earlier methods, there are five modulation signals: three sinusoidal references and two ST envelopes. ST occurs when the peak of the carrier wave is greater than V_p or less than V_n. Otherwise, the inverter is operated as in traditional SPWM control.

The variable B is figured out and kept constant by maintaining D_o as constant. The main target of the MCBC is to achieve maximum boost while keeping it constant throughout, which helps to drop the current and voltage ripples that appear in the MBC technique. The frequency of the upper and lower envelops curves is three times the output frequency [8]. There are two half-periods for both curves in a cycle. The ST modulating signals (V_p and V_n) are expressed as the following:

$$V_p = \sqrt{3}M + Msin\left(\theta - \frac{2\pi}{3}\right) \quad 0 \le \theta \le \frac{\pi}{3} \tag{3}$$

$$V_p = Msin\theta \quad \frac{\pi}{3} \le \theta \le \frac{2\pi}{3} \tag{4}$$

$$V_n = Msin\left(\theta - \frac{2\pi}{3}\right) \quad 0 \le \theta \le \frac{\pi}{3} \tag{5}$$

$$V_n = Msin\theta - \sqrt{3}M \quad \frac{\pi}{3} \le \theta \le \frac{2\pi}{3} \tag{6}$$

The duty ratio of the ST is still constant since the distance between V_p and V_n curves is always constant and equal $\sqrt{3}$ m.

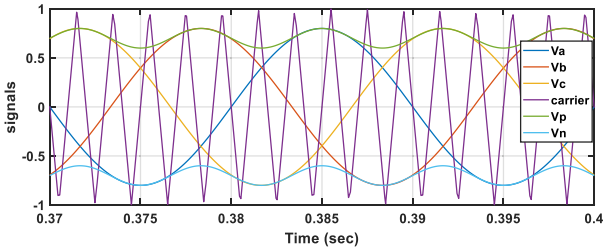

FIGURE 16. Description of the SBPWM.

4) CONSTANT BOOST WITH THIRD HARMONIC INJECTION

The MCBC method described above can be modified by a third harmonic injection [31]. Where the three sinusoidal signals of the phase voltage are injected by a third harmonic component with a value equal to $\frac{1}{6}$ of the fundamental signal, as in Fig. 17. At $\frac{\pi}{3}$ the value of V_a reaches ($\frac{\sqrt{3}}{2}m$), which is the maximum possible value, while V_b is at the lowest value, which is equal to ($-\frac{\sqrt{3}}{2}m$). Therefore, to control the ST time using 3rd HI, only two DC voltages (V_p and V_n) are needed. Thus, it corresponds to the MCB control method in calculating the voltage gain. The difference is that the modulation index m is larger, which increased from one to ($\frac{2}{\sqrt{3}}$). The voltage gain G can be varied from (0 to ∞) smoothly by changing the value of m.

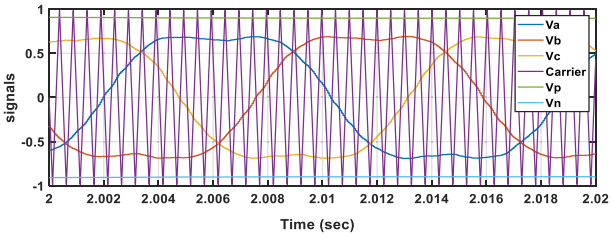

FIGURE 17. Description of the THI-CBPWM.

5) MODIFIED SPACE VECTOR CONTROL (MSVC) [28]

Space vector pulse width modulation (SVPWM) technology is commonly used because of the higher modulation index

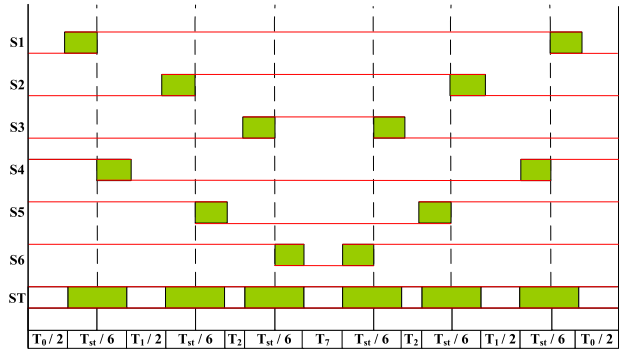

FIGURE 18. Description of MSVPWM.

TABLE 5. Comparison of modified PWM techniques [24].

Type	SB PWM	MB PWM	MCB PWM	3rdHI MCBC	MSV PWM
D_o	$1-M$	$\frac{2\pi-3\sqrt{3}M}{2\pi}$	$\frac{2-\sqrt{3}M}{2}$	$1-\sqrt{3}\frac{M}{2}$	$\frac{2\pi-3\sqrt{3}M}{2\pi}$
B	$\frac{1}{2M-1}$	$\frac{\pi}{3\sqrt{3}M-\pi}$	$\frac{1}{\sqrt{3}M-1}$	$\frac{1}{\sqrt{3}M-1}$	$\frac{\pi}{3\sqrt{3}M-\pi}$
G	$\frac{M}{2M-1}$	$\frac{\pi M}{3\sqrt{3}M-\pi}$	$\frac{M}{\sqrt{3}M-1}$	$\frac{M}{\sqrt{3}M-1}$	$\frac{\pi M}{3\sqrt{3}M-\pi}$
Vs	$(2G-1)V$	$\frac{3\sqrt{3}G-\pi}{\pi}V$	$(\sqrt{3}G-1)V$	$(\sqrt{3}G-1)V$	$\frac{3\sqrt{3}G-\pi}{\pi}V$
M	1	1	1	$\frac{2}{\sqrt{3}}$	$\frac{2}{\sqrt{3}}$

MBC and MSVPWM have the largest voltage gain at a given M, followed by CBC, 3rd HI-CBC, and finally SBC. Also, in the case of the same voltage gain factor G, MBC and MSVPWM have less voltage stress above the switches than SBC and CBC.

bands ($0 \leq m \leq \frac{2}{\sqrt{3}}$) in the linear region. Compared to SPWM, it supplies lower current harmonics. It has eight space vectors (six active vectors) and (seven null vectors). For ZSI, MSVPWM is used to obtain ST states as part of the switching pattern. The ST periods are included during the periods of null vectors of the total period T_n, while the active state times T_1, T_2 and T_Z are unchanged, as seen in Fig. 18.

Two types of MSVPWM can be used. The first pattern is based on the partial conversion of null states to ST states. In this pattern, the ST period of T_o is limited to $\frac{3}{4}$ of the period of the null state T_n. That is, null states are not completely used as an ST. This limits the achievement of higher values of gain. Therefore, it has been modified into the second pattern, where zero states are completely converted to ST. Thus, the gain of this pattern is higher than the gain of the first pattern.

Although MB-PWM has the highest voltage gain rate and boost ratio. However, it is not suitable for PV applications. Because the ST duty ratio is determined by the MPPT algorithm which targets the DC reference voltage at the maximum possible power output is achieved. CBPWM or MSVPWM is preferred because they achieve a relatively high gain and an appropriate voltage boost ratio and are suitable for PV applications.

TABLE 6. Advantages and disadvantages of PWM techniques [27].

Name	Advantages	Disadvantages
SB PWM	• V_c ripple is low. • High peak voltage across bridge switches for same operating point. • Low impedance network size.	• Much higher V_{stress} on switches. • Lower G factor for given M. • Much higher switching losses due to higher $V_{dc-link}$.
MB PWM	• Lowest V_{stress} for the same V_{out} but with a variable D_{ST}. • Introduces low switching losses. • Largest G factor for any M. • Useful for high-speed motor drives due to high frequency.	• Not suitable for PV systems, due to variable D_{ST}. • Low-frequency ripples in dc-side, which increases capacitor size. • High impedance network size. • High THD in output.
MCB PWM	• Relatively lower THD in load current. • Most G and constant D_{ST}. • Switching losses less than MSVC & SBC but higher than MBC. • Normal impedance network size.	• Slightly higher V_{stress}, but with constant D_{ST}. • Complex to implement. • Low peak voltage at same operating point. • V_C ripple is slightly higher.
MSV PWM	• Low impedance network size. • Largest G factor for any M. • Higher M. ($0 \leq M \leq \frac{2}{\sqrt{3}}$) in linear region.	• High V_{stress}, with constant D_{ST}. • Switching losses higher than MB. • High THD in output. • Large oscillations in both V_C & V_{in}.

IV. CONTROL STRATEGIES FOR GRID CONNECTED SYSTEMS

The task of a grid-connected PV system is to convert DC power produced by the PV array into AC power that can be fed into the grid. Thus, the control unit design aims to provide the maximum power from the PV arrays with the desired power factor and low harmonic distortion (THD) in the output. The designed controller must follow the reference and be able to reject disturbances. To implement a good ZSI behavior control strategy, it is necessary to formulate a good dynamic model of the inverter. Several small-signal analyses and mathematical models have been presented in the literature to study the overall system's performance.

Meanwhile, mathematical models have been presented in the literature to study the system's dynamic behavior, which can be used in control strategies [23], [26], [66], [67], [68], [69], [70], [71], [72], [73], [74], [75], [76], [77]. In general, M and Do are the primary control variables in ZSI. Meanwhile, the capacitor voltage or DC-link voltage and the output voltage of the inverter must be controlled. The inductor's internal resistance and the capacitor's equivalent series resistance also influence the dynamics of the impedance source networks and thus are taken into consideration while modeling the small-signal [67], [68], [69], [70]. Parameter values affect system performance, so designers try to choose component values and consider design constraints [12], Table 7 shows the result of changing the values

TABLE 7. Changing the parameter effect values on the system [12].

Parameters change		Effect on system dynamics			
Item	Change	Settling time	Natural frequency	System damping	Other
L	Increase	Increase	Decrease	Decrease	• Increase phase deficit to less than minimum. • Increase oscillatory response.
C	Increase	Increase	Decrease	Increase	• Increase rise time.
D_o	Increase	Increase	Decrease		• Increase phase deficit to less than minimum.
R_c	Increase			Increase	• Increase phase deficit to less than minimum. • Increase current ripple in C.
r_L	Increase			Increase	• Increase phase deficit to less than minimum. • Increase voltage ripple across L.

of these parameters on system dynamics, such as feedback control bandwidth, ripple content, component size and cost, damping factor, resonance frequency, and output matching for the required voltage. Several control methods have been proposed in the literature to achieve the desired performance and control the DC-link voltage and AC output voltage of the impedance source inverters [28], [29], [31], [32], [33], [34], [71] [78], [79], [80], [81], [82], [83], [84], [85], [86], [87], [88], [89], [90], [91], [92], [93], [94], [95], [96], [97]. In all these control methods, there are two control degrees of freedom (D_o and M). The DC-link voltage is controlled by the ST duty ratio Do and the modulation index M controls the output voltage.

In several recent publications, feedback control strategies for the impedance network inverters captured researchers' attention [28], [29], [31], [32], [33], [34], [71] [78], [79], [80], [81], [82], [83], [84], [85], [86], [87], [88], [89], [90], [91], [92], [93], [94], [95], [96], [97]. It compares the output parameters like voltage and current of the inverter and the input parameter like DC-link voltage with the reference values to produce a three-phase sinusoidal reference signal. Based on this signal and the ST duty ratio signal (D_o), the MPPT controller provides the necessary pulses to switch the IGBTs in the inverter H-bridge using PWM technology, as mentioned in [41]. The general diagram of the different control parts used in the grid PV system is shown in Fig. 19. They are summarized as follows:

- The DC side control aims to boost the DC-link voltage (V_{dc}) and maintain it as a constant, the boost ratio (B) is controlled by controlling the ST duty ratio (D_o), and the outer loop control is adopted for controlling the ZSI capacitor voltage (V_c).
- The AC side control converts the DC voltage into AC voltage and achieves the unity power factor. The inner current loop is adopted to ensure that the inverter current can follow the AC grid voltage [78].

A. THE DC CONTROL STRATEGIES

In As mentioned earlier, the PV array voltage is controlled by the ST duty cycle to track the maximum power points. There are four linear methods to control the DC-link voltage (V_{dc}) of ZSI, as shown in Fig. 20, which are:

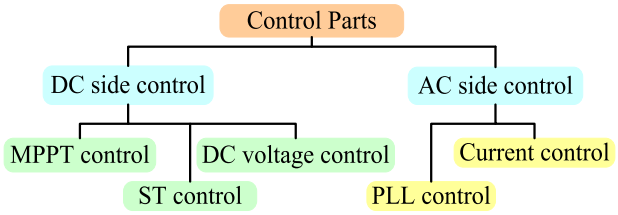

FIGURE 19. Feedback control strategy parts.

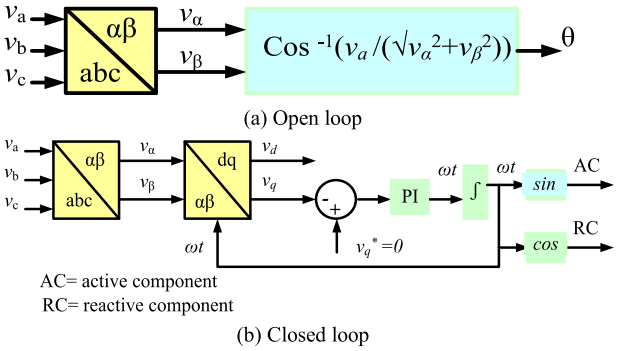

FIGURE 20. DC-link voltage control types of the ZSI [5].

1) CAPACITOR VOLTAGE (V_c) CONTROL [29], [32], [33], [34], [78], [79], [80], [81], [82], [83]

The capacitor voltage is controlled by adjusting the ST duty ratio where a PID controller is used and setting the modulation index to equal $(1 - D_o)$. the gains of the PI controller can be obtained by try and error with saturation or by a neural network to achieve a wide-bandwidth control. In addition, a non-linear control method was used to control the V_c, such as the sliding mode control method, the neural network controllers and so on. Fig. 21. sets out the different non-linear controllers.

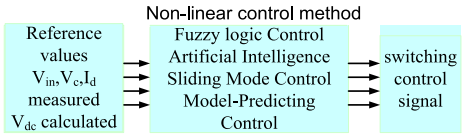

FIGURE 21. Non-linear control methods.

2) INDIRECT CONTROL OF DC-LINK VOLTAGE [83], [84]

A PID-like fuzzy control unit is employed to control the mean value indirectly V_{dc}. In [84], the peak of DC-link voltage (v_{dc}(peak)) is indirectly controlled through controlling the peak of inverter output voltage (v_{ac}) using a PI control unit to adjust M, while Do is calculated by measuring the PV voltage (V_{in}) and comparing it to the desired peak of DC-link voltage (v_{dc}).

3) DIRECT CONTROL OF DC-LINK VOLTAGE [31], [85]

The v_{dc} is directly controlled through the adjusting value of the Do. The v_{dc} value can be measured by an additional

circuit due to its pulsating shape and hence complicating the control algorithm. On the other hand, it can be estimated by measuring V_{in} and V_c, while $v_{dc} = 2V_c - V_{in}$.

4) UNIFIED CONTROL [86], [87]

Unified control is used to simultaneously regulate the modulation index and the ST duty ratio. This is done by controlling the AC output voltage with a single PI control unit. The previous control methods share that they use the single-loop DC-link voltage control technique, where the DC-link voltage is directly affected by the changes in the PV input voltage, while the ST ratio is considered a command signal for the control method. It also suffers from two challenges in the case of high-power inverters.

- Inductor current is uncontrolled and can be overloaded during the transient mode.
- Finite stability limits.

Fig. 22. and Fig. 23. show the scheme of the single control loop (SCL) and the double control loop (DCL) system, respectively [32].

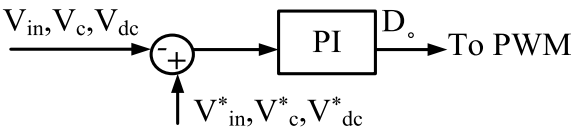

FIGURE 22. Single loop control system.

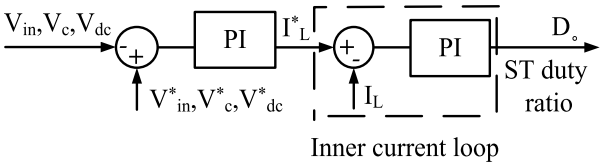

FIGURE 23. Double loop control system.

Therefore, double-loop voltage control in high power inverters is preferred to overcome these drawbacks. it is noted that the input inductor current (I_L) is the command signal for the control method. As shown in Fig. 23, the control process is divided into an inner and outer loop [26]. The inner loop determines the DC-link voltage and ensures instantaneous response while controlling I_L and V_c using a PI controller. On the other hand, the PI control method enhances stability in the outer loop. Table 7 reviews the previous control methods and their characteristics.

B. GRID SIDE CONTROL STRATEGY

The control strategy for the grid side or the AC side is implemented in the *dq*-axis frame, where the three-phase quantities are transformed into a frame of reference with a shunt matrix given in Table 8 [37]. A phase-locked loop (PLL) controller synchronizes the inverter's output current with the grid voltage, thus achieving the unity power factor.

1) PHASED LOCKED LOOP (PLL)

The PPL is needed to know the angle of the grid voltage and hence generate the reference signal with a similar angle. Therefore, the current can be in phase with the grid voltage, as shown in Fig. 24, and hence the unity power factor can be achieved. So, the PLL is used to generate this signal which is used as a reference signal and sent to the current controller.

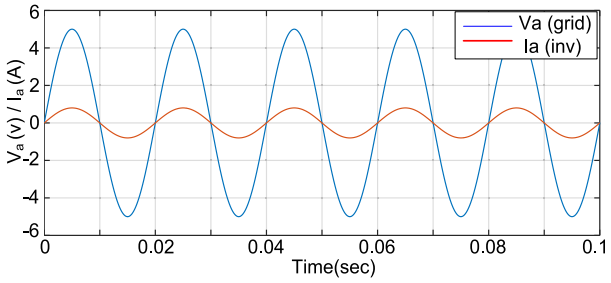

FIGURE 24. Active current signal with the grid voltage.

Similarly, for reactive power control, the PLL is used to generate a signal which is 90° out of phase with the active voltage, as shown in Fig. 25.

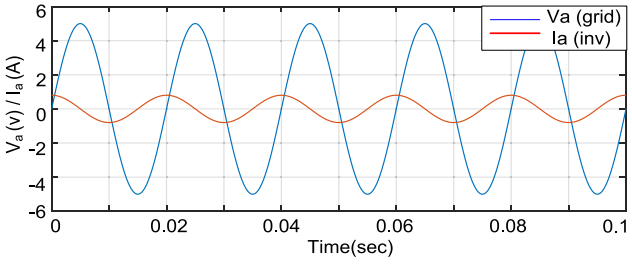

FIGURE 25. Reactive current signal with the grid voltage.

There are two ways to implement the PLL; open-loop and closed-loop.

First Method:

The three-phase voltages (v_a, v_b, v_c) are converted to two-phase voltages (v_α, v_β), and substitute the values for the two voltages (v_α, v_β), in the equation $\theta = \cos^{-1}(v_a/\sqrt{(v_\alpha^2 + v_\beta^2)})$, angle information (θ) can be obtained, which in turn is used to generate the reference signal for current in both the active and the reactive power, as shown in Fig. 26(a). Nevertheless, this method is not used in many situations due to some drawbacks such as:

- The algebraic method with the simple mathematical operation.
- The open-loop system makes the system prone to go into unstable situations and critical network conditions.
- This PLL cannot withstand surges, harmonics, noises, and spikes.
- Drift the angle, which means that PLL output may produce wrong angle information.

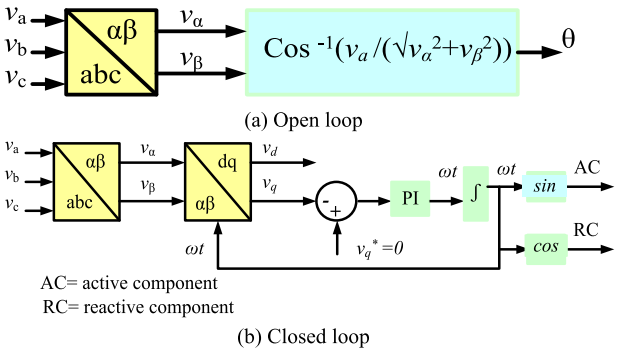

FIGURE 26. PLL method.

Second Method:

Also like the previous method, starting by converting three-phase voltages in the normal frame (v_a, v_b, v_c) into a two-phase voltage in the stationary frame (v_α, v_β), and then to a two-phase voltage in a synchronous frame (v_d, v_q), as shown in Fig. 26(b), which shows the closed-loop PLL method, also Fig. 27(a), which shows the phasor diagram of the (α, β) axis, grid voltage, (d, q) axis, and the angle ωt, which is the angle between d-axis and (α) component.

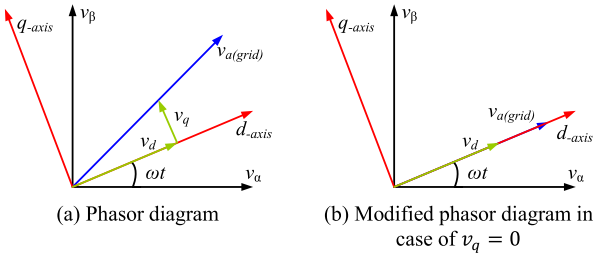

FIGURE 27. PLL Theory.

The phasor diagram shows that the d-axis does not completely align with the grid voltage, so non-zero values of the voltages of the d-axis and q-axis appear. But using some control mechanism, the q-axis voltage goes to equal zero, which will adjust the phasor diagram so that the grid voltage aligns perfectly with the d-axis. The new phasor diagram is shown in Fig. 27(b).

It is clear from the modified phasor diagram that the d-axis voltage and the q-axis voltage are equal to zero, and the angle (ωt) is changed to a new value. This new value of the angle (ωt) can be used to generate the active and reactive components.

From the PLL scheme, the PI controller is used to keep the q-axis voltage equal to zero, so the reference value of the q-axis voltage must be zero. The output of the PI controller is sent to an integrator to find the angle (ωt) and finally use the (sin and cos) functions to generate the active and reactive components, which are the final output of the PLL where the active component is aligned in phase with the d-axis, and the reactive component is aligned in phase with the q-axis.

2) TWO-LOOPS CONTROL STRATEGY

Usually, a double-loop or two-loops control strategy is used: [37]

- The inner control loop in current that adjusts the grid current ensures power quality, current protection, and the function of harmonic compensation and dynamics.
- The outer control loop in voltage controls the DC-link voltage and works to balance the power flow through the inverter. It aims to maintain system stability with slow dynamics.

However, other control strategies have been used in the different literature, such as:

- The current injected into the grid is indirectly controlled in the outer control loop for DC-link voltage with an inner control loop in power.
- The outer control loop is in power with an inner control loop in the current.

But all previous control strategies can be implemented with three frames of reference:

- The synchronous frame,
- The fixed frame,
- The normal frame.

The control carried out through these frames of reference is shown in Fig. 28(a, b, c).

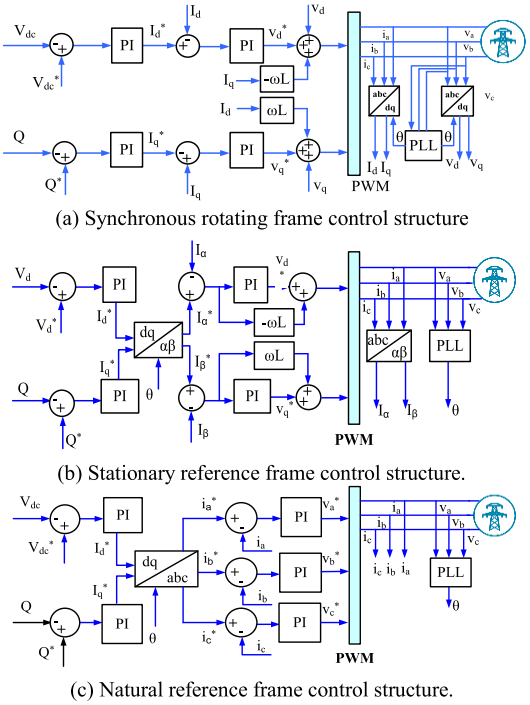

FIGURE 28. Reference frames control. [38].

3) CONTROL REQUIREMENTS

Generally, a PI controller with grid voltage feedforward is used for current-controlled PV inverters, [38] but this method has the following drawbacks:

- A steady-state error occurs when the PI controller traces the sinusoidal reference.
- The system's ability to reject disturbance is poor due to a bad integrator performance.

Therefore, two methods have been proposed to bypass these shortcomings, which are:

- Generalized integration: This means using a double integrator that achieves infinite gain at a certain frequency, called the resonant frequency, and thus, can be used as a notch filter to compensate for harmonics in a highly selective manner. [12]
- P + resonance controller: A stationery frame regulator is used, and the PI controller used as a DC compensator is converted into an equivalent AC compensator having the same frequency response characteristics at the desired bandwidth. [39]

4) DECOUPLING CONTROL OF THE CURRENT LOOP

In Fig. 29(a), if v_{ao}, v_{bo}, v_{co}, are the output voltages of the inverter and were V_a, V_b, V_c, are the three-phase voltages of the grid, $L_a = L_b = L_c$ and they are the inductances of the line filter, $r_a = r_b = r_c$ are the internal resistances of the inductors, and finally i_a, i_b, i_c are the inverter output currents. The voltage equations in the normal (a, b, c) frame of reference can be formulated as follows [65]:

$$\left.\begin{aligned} V_a &= V\cos(\omega t) = -L\frac{di_a}{dt} + v_{ao} - r_a i_a \\ V_b &= V\cos(\omega t - \frac{2\pi}{3}) = -L\frac{di_b}{dt} + v_{bo} - r_b i_b \\ V_c &= V\cos(\omega t + \frac{2\pi}{3}) = -L\frac{di_c}{dt} + v_{co} - r_c i_c \end{aligned}\right\} \quad (7)$$

where V is the peak voltage of the grid phase and ω is the angular frequency. The previous equations can be converted to dq synchronous frame of reference as follows:

$$\left.\begin{aligned} V_d &= L\frac{di_d}{dt} - \omega L i_q + r_d i_d + v_d \\ V_q &= L\frac{di_q}{dt} - \omega L i_d + r_q i_q + v_q \end{aligned}\right\} \quad (8)$$

We can find that in the d-q frame, the current is coupled in the d-q axis, which brings difficulty in the design of the controller. Therefore, it is necessary to obtain a method for separating or decoupling the control [9]. Suppose:

$$\left.\begin{aligned} V_d &= v_d - \omega L i_q + \Delta v_d \\ V_q &= v_q - \omega L i_d + \Delta v_q \end{aligned}\right\} \quad (9)$$

Thus, we get:

$$\left.\begin{aligned} \Delta v_d &= L\frac{di_d}{dt} + r_d i_d \\ \Delta v_q &= L\frac{di_q}{dt} + r_q i_q \end{aligned}\right\} \quad (10)$$

Using the PI controller, the equation can be formulated as follows:

$$\left.\begin{aligned} \Delta v_d &= (K_p + \frac{K_i}{S})(i_d^* - i_d) \\ \Delta v_q &= (K_p + \frac{K_i}{S})(i_q^* - i_q) \end{aligned}\right\} \quad (11)$$

where K_p is a proportional gain and K_i is an integral gain of PI controller. Substituting (42) into (43) we get the following matrix:

$$\begin{bmatrix} \frac{di_d}{dt} \\ \frac{di_q}{dt} \end{bmatrix} = \begin{bmatrix} \frac{-R + (K_p + \frac{K_i}{S})}{L} & 0 \\ 0 & \frac{-R + (K_p + \frac{K_i}{S})}{L} \end{bmatrix} \begin{bmatrix} i_d \\ i_q \end{bmatrix} + \frac{(K_p + \frac{K_i}{S})}{L} \begin{bmatrix} i_d^* \\ i_q^* \end{bmatrix} \quad (12)$$

This realizes the process of controlling the current loop disconnection. As shown in Fig. 29-b.

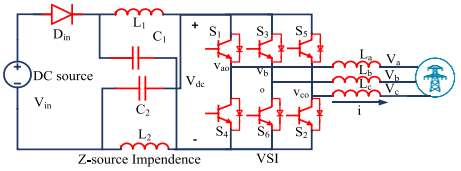

(a) GCPVSs based on ZSI

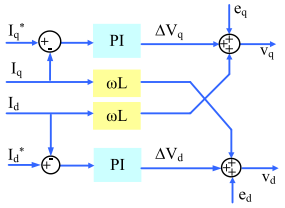

(b) Current control loop [68].

FIGURE 29. Decoupling control of the current loop. [38].

5) ACTIVE AND REACTIVE POWER CONTROL

Active and reactive power control is critical in a grid-connected PV system. Generally, all the radiation absorbed from the PV array is converted into active power by the grid-connected PV system and is taken away from reactive power generation. This gives designers and users the ability to control the system and adjust its performance easily. However, the widespread development in grid-connected PV systems, especially in places far from the main grids or those connected to sub-grids only, has made reactive power compensation and harmonic tuning another major consideration. The three-phase inverter circuit can be compatible with the three-phase reactive power compensator. It can output reactive power and reduce current distortion to the grid by appropriate control of the inverter currents [60], [61].

Some studies have combined ZSI with reactive power compensation or harmonic tuning. The firing time has

been combined with sinusoidal pulse width modulation (SPWM) [62], [63]. A standardized grid-connected photovoltaic system control with reactive power compensation and harmonic tuning based on ZSI has been proposed [64].

6) ANALYSIS OF ACTIVE AND REACTIVE POWER OF PV SYSTEM

Fig. 30. shows the Thevenin equivalent circuit for the grid-connected PV system where the $Z_g = X_g + R_g$ is the equivalent impedance of the grid side [60].

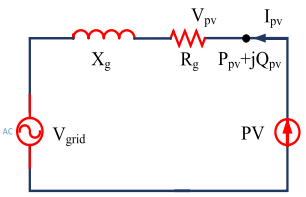

FIGURE 30. Thevenin equivalent circuit of grid-connected PV system.

When the unity power factor is adopted to control the PV system, the grid voltage V_{pv} changes to ΔV_{pv}, so the identical current also changes to ΔI_{pv} as follow:

$$\Delta V_{pv} = \Delta I_p(R_g + jX_g) = \frac{\Delta P_{pv} V_{pv}(cos\emptyset + jsin\emptyset)}{S_k} \quad (13)$$

where, ΔP_{pv} is the change in PV output active power, V_{pv} is the rated voltage at the point of common coupling (PCC), S_K is the short circuit capacity, Q is the equivalent impedance angle, and ΔI_p is the change in the active current of the PV system. According to the previous equation, when the PV output is greater than a certain value, the PCC voltage is higher than the normal values. Furthermore, when the PV system is connected to the reactive power voltage control mode, the change in the grid voltage can be expressed by:

$$\Delta V_{pv} = \frac{\Delta S_{pv} V_{pv}[cos(\emptyset + \theta) + jsin(\emptyset + \theta)]}{S_k} \quad (14)$$

where, ΔS_{pv} is the change in active power generated by the PV system , θ is the power factor angle of the system connected to the PV grid, and ΔI_q is the change in the reactive current in the PV system, from (46), the path of change is shown in the Fig. 31.

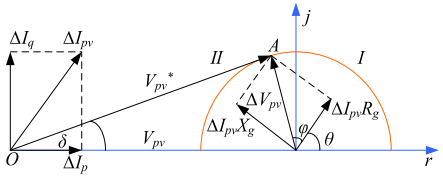

FIGURE 31. Vector analysis diagram for voltage change caused by the PV system.

As per Fig. 31, when the PV output active power is increased, the ΔV_{pv} is at the top of the x-axis. This means that the grid-connected inverter's reactive power can be regulated and keep the PCC voltage constant. When ΔV_{pv} at point A in Fig. 34., the V_{pv} will equal $V_{pv}*$. Therefore, the grid-connected PV system must fully use the inverter's reactive power control to implement reactive power and voltage regulation [60]

7) ACTIVE AND REACTIVE POWER CONTROL OF ZSI

Relying on the instantaneous power theory, the relation of instantaneous active power p and reactive power q with grid voltage V_d and V_q can be formulated in the synchronous frame of reference (d – q) as follow [63], [64]:

$$\left.\begin{aligned} P &= \frac{3}{2}(V_d I_d + V_q I_q) \\ q &= \frac{3}{2}(V_d I_q + V_q I_d) \end{aligned}\right\} \quad (15)$$

where I_d and I_q does ZSI produce the active and reactive output currents. Since the grid voltage q is zero, (15) can be simplified to

$$\left.\begin{aligned} P &= \frac{3}{2} V_d I_d \\ q &= \frac{3}{2} V_d I_q \end{aligned}\right\} \quad (16)$$

So, the active and reactive power of the ZSI can be controlled by adjusting the active current I_d and reactive current I_q produced by ZSI in a synchronous frame of reference. The ZSI mathematical model can be formulated as mentioned before in equations (9) and (10), which means that the inverter output currents I_d and I_q can be controlled separately from the reference current signals I_d^* and I_q^* as shown in Fig. 31. Finally, the active and reactive power of ZSI can be controlled.

V. CHALLENGES AND FUTURE DIRECTIONS

From the above it is clear that achieving all the advantages and overcoming all the disadvantages through one ISN design is impossible. Hence, several models have been proposed to complement the shortcomings of ZSI topologies depending on the intended application. The main challenges are increasing efficiency and reducing the system's overall cost. But the efficiency of the inverter requires a balance between increasing the advantages and reducing the disadvantages, for example, increasing the gain factor to the extent that the switches withstand voltage stress without damage. From the above, the passive components, such as capacitors and inductors, are the major contributors to the total cost of inverter design. The performance of the inverter is also closely related to the number of switches used in the design. Hence, a trade-off must be ensured while forming the impedance network with active and passive components.

Moreover, the control techniques used in the system, will greatly affect the performance of the inverter in terms of losses. Therefore, in future work, researchers can use the active component based on GaN and SiC, which may reduce

TABLE 8. Review of previous ZSI control strategies.

Control method	Controller type	Sense Signal	Control variable	Drawbacks	Ref.
V_c control (indirect)	SCL + PID	V_c	D_o	• Controller is designed based on a second order model. • Modified simple boost control is implemented. • Consider dynamics of impedance network only.	[78]
	SCL + PID	VM mode: V_c and V_{in}		• Estimate $V_{dc\text{-}link}$ by measuring V_C and V_{in}. • V_{in} controller small- signal model • Good input and load disturbance rejection.	[98]
	SCL + PI with saturation	V_c, v_o (a, b, c)	$D_\circ$	• Controller is not designed.	[99]
	SCL + PI	V_c, v_o (a, b, c)	$D_\circ$	• Controller is designed by ANN. • Capacitor voltage is linearly controlled by $K = \frac{V_c}{V_{in}}$. • Enhances disturbance rejection from load and input variations.	[81]
	SCL nonlinear (gain scheduling + state feedback) control	V_c, v_o (a, b, c)	$D_\circ$& M	• Complicated control algorithm. • Controller is very stable in steady state operation. • Not suitable for rapidly varying reference point.	[26], [27], [28]
	MCL+ P for inner current and PI for outer voltage loop	V_c, i_L, V_{cf} (a, b, c), i_c f (a, b, c)	$D_\circ$& M	• Mitigate transfer of dc-side disturbance to ac side. • Excellent reference tracking • rejection of disturbances arising from input and output sides	[29], [34]
	DLC + PI	V_c, V_{in} and i_L	$D_\circ$	• Controller is not designed or tuned by ANN. • Achieves better steady and transient performance and stability compared to single-loop control. • Enhances disturbance rejection	[29], [30], [31]
		CPM mode: V_c, V_{in} and i_L		• Increases the phase margin and offers simple compensator design	[79]
Indirect V_{dc} control	SCL + PID fuzzy controller	$V_{dc-link}$	$D_\circ$	• Controller is inaccurate due to non-linear relation between V_c and V_{dc}. • Controller is not designed. • Modified simple boost control is implemented • Improve transient response • Enhances disturbance rejection • Simplifies controller design	[32]
	SCL + PI with saturation	$V_{dc-link}$	M	• ST is not controlled. • controller is not designed.	[33]
Direct V_{dc} control	*SCL + PID*	$V_{dc-link}$	$D_\circ$	• Extrinsic complicated sensing circuit. • Controller is not designed.	[34], [81]
	DCL + PI	$V_{dc-link}$	$D_\circ$& M	• Modified simple boost control is implemented. • Improves transient response. • Enhances disturbance rejection. • Simplifies controller design.	[35]
	DCL+PI for outer V_{dc} loop, and P for inner current loop.	$V_{dc-link}$	$D_\circ$	• A simple control of the ZSI.	[36]
Unified control		$v_{o(a, b, c)}$	V^* with MSVM	• Controller is not designed. • Used for isolated loads.	[37]

TABLE 8. *(Continued.)* **Review of previous ZSI control strategies.**

		$v_{o(a,b,c)}$	D_o & M	• Controller designed from large-signal model of converter. • Stable and robust to large parameter, line, and load variations. • Fast response, less current ripple when subject to large load/source variations. • Complex control algorithm	[86]
Indirect V_{in} control	SCL + PI with saturation	v_{in} and v_o	D_o	• Simple and easy to implement. • Performs rough regulation. • Did not consider the impact of impedance network (RHP pole etc.) in stability.	[33]
Indirect v_{in}, i_{in}, v_o, i_o	SCL + PI	v_{in}, i_{in}, $v_{o(a,b,c)}$ and $i_{o(a,b,c)}$	D_o	• Low cost and ease of digital implementation. • Battery-assisted QZSI control which controls the state of charge (SOC) of the battery and the power injected into the grid.	[86]
	Sliding mode (SM) control	v_{in}, i_{in}, $v_{o(a,b,c)}$	D_o & M	• Controller designed from large-signal model of converter. • Stable and robust to large parameter, line, and load variations. • Fast response with less current ripple when subject to large load/source variations. • Complex control algorithm.	[32], [77], [78]

TABLE 9. **A summary of the reference frames used for grid-side control. [37].**

Feature(s)	Synch. Reference frame	Stationary reference frame	Natural reference frame
Transformation	dq0	$\alpha\beta 0$	abc
Control variables	DC	Sinusoidal	1φ, 3φ variables
Controller(s)	PI	PR	(PI, PR, hysteresis)
Controller characteristics	Suitable for DC	• Suitable to sinusoidal quantity. • High gain at ωr, ess=0	Suitable for AC
Grid phase angle extraction	PLL & arctangent function	PLL & arctangent function	PLL & arctangent function
Modulation necessary	Yes, for switching the power devices.	Yes, for switching the power devices.	No, power devices are switched directly.
Evaluation	• Voltage feedforward is requisite for cross coupling. • θ is requisite for estimate.	• Uncomplicated control. • θ is not requisite.	• Extremely complex control. • θ is not requisite. • Separate control of each phase.

component losses and improve the efficiency, reliability, and power density of these inverters. Accordingly, the expansion of this work can be predicted by considering the following objectives:

- Work on developing impedance source network models in terms of boost factor, the voltage stress on components, the total number of devices, and most importantly, inverter efficiency.
- Replacing two-stage inverters with ISNs reduces converter loss and improves the reliability and power quality of the whole system.

VI. CONCLUSION AND PERSPECTIVES

Since the first model of ISNs appeared, wide areas of research have opened up for many improvements and modifications to the inverter chassis models. In this review, an overview of

several models of impedance source network inverters developed from the original ZSI or semi-ZSI format is presented. In fact, although it has not received enough attention, the EB-QZSI inverter has many advantages in the field of energy conversion, and they are summarized in Table No. four. This review also provided a compilation of the modified PWM techniques to suit impedance source network inverters that have been addressed in the literature with their applications and advantages for specific goals and objectives for their essential role in improving inverter performance. Hence, the study concluded that MCBC and MSVC may be the best performers in terms of ST work ratio, effort gain, and reinforcement ratio.

Finally, the study presented a proposal for an integrated inverter input and output control technology. Including DC-link voltage control methods, current control techniques, in addition to clarifying the concept of decoupling control in order to achieve the best performance of the grid connected system.

ACKNOWLEDGMENT

The authors would like to thank the support of Prince Sultan University for paying the Article Processing Charges (APC) of this publication.

REFERENCES

[1] O. Ellabban and H. Abu-Rub, "Z-source inverter: Topology improvements review," *IEEE Ind. Electron. Mag.*, vol. 10, no. 1, pp. 6–24, Mar. 2016.

[2] H. Chen and H. Zhao, "Review on pulse-width modulation strategies for common-mode voltage reduction in three-phase voltage-source inverters," *IET Power Electron.*, vol. 9, no. 14, pp. 2611–2620, Nov. 2016.

[3] T. E. Shults, O. O. Husev, and J. G. Zakis, "Overview of impedance source networks for voltage source inverters," in *Proc. 16th Int. Conf. Young Spec. Micro/Nanotechnol. Electron Devices*, Jun. 2015, vol. 65, no. 7, pp. 5456–5465.

[4] M.-K. Nguyen, Y.-C. Lim, and Y.-G. Kim, "TZ-source inverters," *IEEE Trans. Ind. Electron.*, vol. 60, no. 12, pp. 5686–5695, Dec. 2013.

[5] Y. Liu, H. Abu-Rub, and B. Ge, "Z-source/quasi-Z-source inverters: Derived networks, modulations, controls, and emerging applications to photovoltaic conversion," *IEEE Ind. Electron. Mag.*, vol. 8, no. 4, pp. 32–44, Dec. 2014.

[6] P. C. Loh, F. Gao, and F. Blaabjerg, "Embedded EZ-source inverters," *IEEE Trans. Ind. Appl.*, vol. 46, no. 1, pp. 256–267, Jan. 2010.

[7] V. F. Pires, A. Cordeiro, D. Foito, and J. F. Martins, "Quasi-Z-source inverter with a T-type converter in normal and failure mode," *IEEE Trans. Power Electron.*, vol. 31, no. 11, pp. 7462–7470, Nov. 2016.

[8] W. Qian, F. Z. Peng, and H. Cha, "Trans-Z-source inverters," *IEEE Trans. Power Electron.*, vol. 26, no. 12, pp. 3453–3463, Dec. 2011.

[9] M. Adamowicz, R. Strzelecki, F. Z. Peng, J. Guzinski, and H. A. Rub, "New type LCCT-Z-source inverters," in *Proc. EPE*, Sep. 2011, pp. 1–10.

[10] P. C. Loh, D. Li, and F. Blaabjerg, "Γ-Z-source inverters," *IEEE Trans. Power Electron.*, vol. 28, no. 11, pp. 4880–4884, Nov. 2013.

[11] X. Wang and J. Zhang, "Neutral-point potential balancing method for switched-inductor Z-source three-level inverter," *J. Electr. Eng. Technol.*, vol. 12, no. 3, pp. 1203–1210, May 2017.

[12] Y. P. Siwakoti, F. Z. Peng, F. Blaabjerg, P. C. Loh, and G. E. Town, "Impedance-source networks for electric power conversion. Part II: A topological review," *IEEE Trans. Power Electron.*, vol. 30, no. 2, pp. 699–716, Mar. 2015.

[13] S. Bayhan, P. Kakosimos, and H. Abu-Rub, "Model predictive control of five-level H-bridge neutral-point-clamped qZS inverter," in *Proc. 42nd Annu. Conf. IEEE Ind. Electron. Soc.*, Oct. 2016, pp. 5971–5976.

[14] T. Li and Q. Cheng, "A comparative study of Z-source inverter and enhanced topologies," *CES Trans. Electr. Mach. Syst.*, vol. 2, no. 3, pp. 284–288, Sep. 2018.

[15] Y. P. Siwakoti, P. C. Loh, F. Blaabjerg, and G. E. Town, "Y-source impedance network," *IEEE Trans. Power Electron.*, vol. 29, no. 7, pp. 3250–3254, Jul. 2014.

[16] S. Mishra, R. Adda, and A. Joshi, "Inverse Watkins–Johnson topology-based inverter," *IEEE Trans. Power Electron.*, vol. 27, no. 3, pp. 1066–1070, Mar. 2012.

[17] M.-K. Nguyen, Y.-C. Lim, J.-H. Choi, and Y.-O. Choi, "Trans-switched boost inverters," *IET Power Electron.*, vol. 9, no. 5, pp. 1065–1073, 2016.

[18] A. A. Hakim, "Modulation schemes of the three-phase impedance source inverters—Part I: Classification and review," *IEEE Trans. Ind. Electron.*, vol. 65, no. 8, pp. 6309–6320, Aug. 2018.

[19] Z. Zhao, A. M. Elgendy, M. Armstrong, and M. Muhammad, "Constant boost control with third harmonic injection for quasi-Z source inverter used in PV grid-connected system," in *Proc. 21st Eur. Conf. Power Electron. Appl.*, Sep. 2019, pp. 1–9.

[20] Y. Liu, H. Abu-Rub, B. Ge, F. Blaabjerg, O. Ellabban, and P. C. Loh, *Impedance Source Power Electronic Converters*, 1st ed. Hoboken, NJ, USA: Wiley, 2016, pp. 22–75.

[21] F. Z. Peng, M. Shen, and Z. Qian, "Maximum boost control of the Z-source inverter," *IEEE Trans. Power Electron.*, vol. 20, no. 4, pp. 833–838, Jul. 2005.

[22] M. Shen, J. Wang, A. Joseph, F. Z. Peng, L. M. Tolbert, and D. J. Adams, "Constant boost control of the Z-source inverter to minimize current ripple and voltage stress," *IEEE Trans. Ind. Appl.*, vol. 42, no. 3, pp. 770–778, May/Jun. 2006.

[23] Y. Liu, B. Ge, F. J. T. E. Ferreira, A. T. De Almeida, and H. Abu-Rub, "Modeling and SVPWM control of quasi-Z-source inverter," in *Proc. 11th Int. Conf. Elect. Power Quality Utilisation*, Oct. 2011, pp. 1–7.

[24] O. Ellabban, J. Van Mierlo, and P. Lataire, "Comparison between different PWM control methods for different Z-source inverter topologies," in *Proc. 13th Eur. Conf. Power Electron. Appl. (EPE)*, Barcelona, Spain, Sep. 2009, pp. 1–11.

[25] J. Khajesalehi, K. Sheshyekani, M. Hamzeh, and E. Afjei, "Maximum constant boost approach for controlling quasi-Z-source-based interlinking converters in hybrid AC–DC microgrids," *IET Gen. Transmiss. Distrib.*, vol. 10, no. 4, pp. 938–948, 2016.

[26] M. Shen, Q. Tang, and F. Z. Peng, "Modeling and controller design of the Z-source inverter with inductive load," in *Proc. IEEE Power Electron. Spec. Conf.*, Jun. 2007, pp. 1804–1809.

[27] C. Ruqi, Z. Gengshen, G. Tianyong, Z. Ergang, Z. Yao, and Q. Chao, "Modeling and state feedback control of Z-source inverter," in *Proc. 2nd Int. Conf. Power Electron. Intell. Transp. Syst. (PEITS)*, Dec. 2009, pp. 125–129.

[28] A. H. Rajaei, S. Kaboli, and A. Emadi, "Sliding-mode control of Z-source inverter," in *Proc. 34th Annu. Conf. IEEE Ind. Electron.*, Nov. 2008, pp. 947–952.

[29] Q. V. Tran, T. W. Chun, J. R. Ahn, and H. H. Lee, "Algorithms for controlling both the DC boost and AC output voltage of Z-source inverter," *IEEE Trans. Ind. Electron.*, vol. 54, no. 5, pp. 2745–2750, Oct. 2007.

[30] Q. V. Tran, T. W. Chun, H. G. Kim, and E. C. Nho, "Minimization of voltage stress across switching devices in the Z-source inverter by capacitor voltage control," *J. Power Electron.*, vol. 9, no. 3, pp. 335–342, 2009.

[31] H. Rostami and D. A. Khaburi, "Neural networks controlling for both the DC boost and AC output voltage of Z-source inverter," in *Proc. 1st Power Electron. Drive Syst. Technol. Conf. (PEDSTC)*, 2010, pp. 135–140.

[32] X. Ding, Z. Qian, S. Yang, B. Cui, and F. Peng, "A direct DC-link boost voltage PID-like fuzzy control strategy in Z-source inverter," in *Proc. IEEE Power Electron. Spec. Conf.*, Jun. 2008, pp. 405–411.

[33] Y. Tang, S. Xie, and C. Zhang, "Feedforward plus feedback control of the improved Z-source inverter," in *Proc. IEEE Energy Convers. Congr. Expo.*, Sep. 2009, pp. 783–788.

[34] X. Ding, Z. Qian, S. Yang, B. Cui, and F. Peng, "A direct peak DC-link boost voltage control strategy in Z-source inverter," in *Proc. 22nd Annu. IEEE Appl. Power Electron. Conf. Expo. (APEC)*, Feb. 2007, pp. 648–653.

[35] Y. Tang, J. Wei, and S. Xie, "A new direct peak DC-link voltage control strategy of Z-source inverters," in *Proc. 25th Annu. IEEE Appl. Power Electron. Conf. Expo. (APEC)*, Feb. 2010, pp. 867–872.

[36] S. Nema, R. K. Nema, and G. Agnihotri, "Inverter topologies and control structure in photovoltaic applications: A review," *J. Renew. Sustain. Energy*, vol. 3, no. 1, Jan. 2011, Art. no. 012701.

[37] X. Yuan, W. Merk, H. Stemmler, and J. Allmeling, "Stationary-frame generalized integrators for current control of active power filters with zero steady-state error for current harmonics of concern under unbalanced and distorted operating conditions," *IEEE Trans. Ind. Appl.*, vol. 38, no. 2, pp. 523–532, Mar./Apr. 2002.

[38] D. N. Zmood and D. G. Holmes, "Stationary frame current regulation of PWM inverters with zero steady-state error," *IEEE Trans. Power Electron.*, vol. 18, no. 3, pp. 814–822, May 2003.

[39] M. Chuang and L. Hong, "Research on photovoltaic grid-connected control of Z source inverter based on active disturbance rejection technology," in *Proc. IEEE 4th Adv. Inf. Technol., Electron. Automat. Control Conf. (IAEAC)*, Dec. 2019, vol. 6, no. 2, pp. 2648–2652.

[40] J. Zhang, "Unified control of Z-source grid-connected photovoltaic system with reactive power compensation and harmonics restraint: Design and application," *IET Renew. Power Gener.*, vol. 12, no. 4, pp. 422–429, Dec. 2017.

[41] R. Gharakhany, M. Mohamadian, and A. Y. Varjani, "Reactive power compensation using Z-source based photovoltaic system," in *Proc. IEEE Power Energy Soc. Gen. Meeting*, Jul. 2009, pp. 1–7.

[42] J. N. Barath, A. Soundarrajan, S. Stepenko, O. Husev, D. Vinnikov, and M.-K. Nguyen, "Topological review of quasi-switched boost inverters," *Electronics*, vol. 10, no. 12, p. 1485, Jun. 2021.

[43] N. Subhani, R. Kannan, A. Mahmud, and F. Bleiberg, "Z-source inverter topologies with switched Z-impedance networks: A review," *IET Power Electron.*, vol. 14, no. 4, pp. 1–24, Sep. 2020, doi: 10.1049/pel2.12064.

[44] M. Hasan, B. Nozadian, E. Babies, S. H. Hosseini, and E. S. As, "Switched Z-source networks: A review," *IET Power Electron.*, vol. 12, no. 7, pp. 1616–1633, Feb. 2019.

[45] Y. Liu, B. Ge, H. Abu-Rub, and F. Z. Peng, "An effective control method for three-phase quasi-Z-source cascaded multilevel inverter-based grid-tie photovoltaic power system," *IEEE Trans. Ind. Electron.*, vol. 61, no. 12, pp. 6794–6802, Dec. 2014.

[46] A. Lashab, D. Sera, J. Martins, and J. M. Guerrero, "Dual-input quasi-Z-source PV inverter: Dynamic modeling, design, and control," *IEEE Trans. Ind. Electron.*, vol. 67, no. 8, pp. 6483–6493, Aug. 2020.

[47] A. Safari and S. Mekhilef, "Simulation and hardware implementation of incremental conductance MPPT with direct control method using Cuk converter," *IEEE Trans. Ind. Electron.*, vol. 58, no. 4, pp. 1154–1161, Apr. 2011.

[48] A. Ahmad, R. K. Singh, and V. N. Lal, "A family of enhanced voltage gain switched-boost impedance-source inverter topologies for renewable energy resources," in *Proc. IEEE Energy Convers. Congr. Expo. (ECCE)*, Sep. 2019, pp. 4353–4358.

[49] M. M. Haji-Esmaeili, E. Babaei, and M. Sabahi, "High step-up quasi-Z source DC–DC converter," *IEEE Trans. Power Electron.*, vol. 33, no. 12, pp. 10563–10571, Dec. 2018.

[50] P. Liu, H. Wang, Y. Liu, and F. Blaabjerg, "Thermal stress reduction of quasi-Z source inverter drive by model predictive control," *Microelectron. Rel.*, vols. 88–90, pp. 1247–1250, Sep. 2018.

[51] S. Obukhov, A. Ibrahim, and R. Aboelsaud, "Maximum power point tracking of partially shading PV system using particle swarm optimization," in *Proc. 4th Int. Conf. Frontiers Educ. Technol. (ICFET)*, vol. 18, 2018, pp. 161–165.

[52] A. Hintz, U. R. Prasanna, and K. Rajashekara, "Comparative study of the three-phase grid-connected inverter sharing unbalanced three-phase and/or single-phase systems," *IEEE Trans. Ind. Appl.*, vol. 52, no. 6, pp. 5156–5164, Nov. 2016.

[53] S. Bayhan, M. Trabelsi, H. Abu-Rub, and M. Malinowski, "Finite-control-set model-predictive control for a quasi-Z-source four-leg inverter under unbalanced load condition," *IEEE Trans. Ind. Electron.*, vol. 64, no. 4, pp. 2560–2569, Apr. 2017.

[54] S. Bayhan, H. Abu-Rub, and R. S. Balog, "Model predictive control of quasi-Z-source four-leg inverter," *IEEE Trans. Ind. Electron.*, vol. 63, no. 7, pp. 4506–4516, Jul. 2016.

[55] M. Z. I. Sarkar, L. G. Meegahapola, and M. Datta, "Reactive power management in renewable rich power grids: A review of grid-codes, renewable generators, support devices, control strategies and optimization algorithms," *IEEE Access*, vol. 6, pp. 41458–41489, 2018.

[56] B. K. Santhoshi, K. M. Sundaram, S. Padmanaban, J. B. Holm-Nielsen, and K. K. Prabhakaran, "Critical review of PV grid-tied inverters," *Energies*, vol. 12, no. 10, p. 1921, May 2019.

[57] M. K. Nguyen, T. T. Tran, and Y. C. Lim, "A family of PWM control strategies for single-phase quasi-switched-boost inverter," *IEEE Trans. Power Electron.*, vol. 34, no. 2, pp. 1458–1469, Feb. 2019.

[58] A. Kumar, M. Raghuram, S. K. Singh, X. Xiong, and M. Reza, "Analysis and control of enhanced switched boost inverters for wide duty cycle operation," *IEEE Access*, vol. 7, pp. 45427–45439, 2019.

[59] Y. Libin, L. Xin, Z. Ming, T. Yun, Y. Xin, Z. Yutian, S. Danfeng, Y. Xiaochen, and Z. Wei, "A new theory of reactive power control of grid connected PV inverter," in *Proc. Int. Conf. Intell. Transp., Big Data Smart City*, Dec. 2015, pp. 35–38.

[60] W. Libo, Z. Zhengming, and L. Jianzheng, "A single-stage three-phase grid-connected photovoltaic system with modified MPPT method and reactive power compensation," *IEEE Trans. Energy Convers.*, vol. 22, no. 4, pp. 881–886, Dec. 2007.

[61] X. Chen, Q. Fu, D. Infield, and S. Yu, "Modeling and control of Z-source grid-connected PV system with APF function," in *Proc. 44th Int. Univ. Power Eng. Conf. (UPEC)*, Glasgow, U.K., Sep. 2009, pp. 1–5.

[62] S. Khani, L. Mohammadian, S. H. Hosseini, and S. Ghasemzadeh, "Design and control of fully parallel embedded Z-source inverters based flexible photovoltaic systems for grid power quality improvement under distorted condition," in *Proc. 21st Iranian Conf. Electr. Eng. (ICEE)*, Mashhad, Iran, May 2013, pp. 1–7.

[63] K. Q. Qu, Q. Q. Niu, C. Yang, and J. B. Zhao, "Battery charge-discharge control strategy based on the single Z-source three-level SVPWM inverter," in *Proc. IEEE Int. Conf. Appl. Supercond. Electromagn. Devices*, Beijing, China, Oct. 2013, pp. 25–27.

[64] J. Wei, Y. Tang, and S. Xie, "Grid-connected PV system based on the series Z-source inverter," in *Proc. 5th IEEE Conf. Ind. Electron. Appl.*, Jun. 2010, pp. 532–537.

[65] P. C. Loh, D. M. Vilathgamuwa, C. J. Gajanayake, Y. R. Lim, and C. W. Teo, "Transient modeling and analysis of pulse-width modulated Z-source inverter," *IEEE Trans. Power Electron.*, vol. 22, no. 2, pp. 498–507, Mar. 2007.

[66] Y. Li and F. Z. Peng, "AC small signal modeling, analysis and control of quasi-Z-source converter," in *Proc. 7th Int. Power Electron. Motion Control Conf.*, Jun. 2012, pp. 1848–1854.

[67] V. P. Galigekere and M. K. Kazimierczuk, "Small-signal modeling of PWM Z-source converter by circuit-averaging technique," in *Proc. IEEE Int. Symp. Circuits Syst. (ISCAS)*, May 2011, pp. 1600–1603.

[68] T. Lannert, M. Isen, and M. Braun, "Small signal modeling of the quasi-Z-source-inverter and a novel control strategy to minimize the influence of input voltage disturbances," in *Proc. 15th Eur. Conf. Power Electron. Appl. (EPE)*, Sep. 2013, pp. 1–10.

[69] J. Liu, J. Hu, and L. Xu, "Dynamic modeling and analysis of Z source converter—Derivation of AC small signal model and design-oriented analysis," *IEEE Trans. Power Electron.*, vol. 22, no. 5, pp. 1786–1796, Sep. 2007.

[70] Q. Lei, F. Z. Peng, and B. Ge, "Transient modeling of current-fed quasi-Z-source inverter," in *Proc. IEEE Energy Convers. Congr. Expo.*, Sep. 2011, pp. 2283–2287.

[71] O. Ellabban, J. V. Mierlo, and P. Lataire, "A DSP-based dual-loop peak DC-link voltage control strategy of the Z-source inverter," *IEEE Trans. Power Electron.*, vol. 27, no. 9, pp. 4088–4097, Sep. 2012.

[72] C. J. Gajanayake, D. M. Vilathgamuwa, and P. C. Loh, "Small-signal and signal-flow-graph modeling of switched Z-source impedance network," *IEEE Power Electron Lett.*, vol. 3, no. 3, pp. 111–116, Sep. 2005.

[73] F. Guo, L. Fu, C.-H. Lin, C. Li, and J. Wang, "Small signal modeling and controller design of a bidirectional quasi-Z-source inverter for electric vehicle applications," in *Proc. IEEE Energy Convers. Congr. Expo. (ECCE)*, Sep. 2012, pp. 2223–2228.

[74] Q. Lei, S. Yang, F. Z. Peng, and R. Inoshita, "Steady state and transient analysis of a three phase current-fed Z-source PWM rectifier," in *Proc. IEEE Vehicle Power Propuls. Conf.*, Sep. 2009, pp. 426–432.

[75] D. M. Vilathgamuwa, P. C. Loh, and K. Karunakar, "Modelling of three phase Z-source boost buck rectifiers," in *Proc. 7th Int. Conf. Power Electron. Drive Syst.*, Nov. 2007, pp. 1471–1476.

[76] C. L. K. Konga and M. N. Gitau, "Three-phase quasi-Z-source rectifier modeling," in *Proc. 27th Annu. IEEE Appl. Power Electron. Conf. Expo. (APEC)*, Feb. 2012, pp. 195–199.

[77] D. G. Holmes, B. P. McGrath, D. Segaran, and W. Y. Kong, "Dynamic control of a 20 kW interleaved boost converter for traction applications," in *Proc. IEEE Ind. Appl. Soc. Annu. Meeting*, Oct. 2008, pp. 5–9.

[78] X. Ding, Z. Qian, S. Yang, B. Cui, and F. Peng, "A PID control strategy for DC-link boost voltage in Z-source inverter," in *Proc. 22nd Annu. IEEE Appl. Power Electron. Conf. Expo. (APEC)*, Feb. 2007, pp. 1145–1148.
[79] G. Sen and M. E. Elbuluk, "Voltage and current-programmed modes in control of the Z-source converter," *IEEE Trans. Ind. Appl.*, vol. 46, no. 2, pp. 680–686, Mar./Apr. 2010.
[80] O. Ellabban, J. Van Mierlo, and P. Lataire, "Capacitor voltage control techniques of the Z-source inverter: A comparative study," *J. Eur. Power Electron.*, vol. 21, no. 4, pp. 13–24, Dec. 2011.
[81] F. Guo, L. Fu, C.-H. Lin, C. Li, W. Choi, and J. Wang, "Development of an 85-kW bidirectional quasi-Z-source inverter with DC-link feedforward compensation for electric vehicle applications," *IEEE Trans. Power Electron.*, vol. 28, no. 12, pp. 5477–5488, Dec. 2013.
[82] C. J. Gajanayake, D. M. Vilathgamuwa, and P. C. Loh, "Modeling and design of multi-loop closed loop controller for Z-source inverter for distributed generation," in *Proc. 37th IEEE Power Electron. Spec. Conf.*, Jun. 2006, pp. 1–7.
[83] C. J. Gajanayake, D. M. Vilathgamuwa, and P. C. Loh, "Development of a comprehensive model and a multi-loop controller for *Z*-source inverter DG systems," *IEEE Trans. Ind. Electron.*, vol. 54, no. 4, pp. 2352–2359, Aug. 2007.
[84] P. Liu and H. P. Liu, "Permanent-magnet synchronous motor drive system for electric vehicles using bidirectional Z-source inverter," *IET Elect. Syst. Transp.*, vol. 2, no. 4, pp. 178–185, Dec. 2012.
[85] O. Ellabban, J. V. Mierlo, and P. Lataire, "Control of a bidirectional Z-source inverter for electric vehicle applications in different operation modes," *J. Power Electron.*, vol. 11, no. 2, pp. 120–131, Mar. 2011.
[86] S. Yang, X. Ding, F. Zhang, F. Z. Peng, and Z. Qian, "Unified control technique for Z-source inverter," in *Proc. IEEE Power Electron. Spec. Conf.*, Jun. 2008, pp. 3236–3242.
[87] Y. Liu, B. Ge, H. A. Rub, and F. Z. Peng, "Control and design of battery assisted quasi-Z-source inverter for grid-tie photovoltaic power generation," *IEEE Trans. Sustain. Energy*, vol. 4, no. 4, pp. 994–1001, Oct. 2013.
[88] Y. Liu, B. Ge, H. A. Rub, and F. Z. Peng, "An effective control method for quasi-Z-source cascade multilevel inverter-based grid-tie single-phase photovoltaic power system," *IEEE Trans. Ind. Informat.*, vol. 10, no. 1, pp. 399–407, Feb. 2014.
[89] H. A. Rub, A. Iqbal, S. M. Ahmed, F. Z. Peng, Y. Li, and B. Ge, "Quasi-Z-source inverter-based photovoltaic generation system with maximum power tracking control using ANFIS," *IEEE Trans. Sustain. Energy*, vol. 4, no. 1, pp. 11–20, Jan. 2013.
[90] J. H. Park, H. G. Kim, E. C. Nho, and T. W. Chun, "Capacitor voltage control for MPPT range expansion and efficiency improvement of grid-connected quasi-Z-source inverter," in *Proc. IEEE Int. Power Electron. Conf.*, Jun. 2010, pp. 927–931.
[91] D. M. Vilathgamuwa, C. J. Gajanayake, and P. C. Loh, "Modulation and control of three-phase paralleled Z-source inverters for distributed generation applications," *IEEE Trans. Energy Convers.*, vol. 24, no. 1, pp. 173–183, Mar. 2009.
[92] S. J. Amodeo, H. G. Chiacchiarini, and A. R. Oliva, "High-performance control of a DC–DC Z-source converter used for an excitation field driver," *IEEE Trans. Power Electron.*, vol. 27, no. 6, pp. 2947–2957, Jun. 2012.
[93] Z. J. Zhou, X. Zhang, P. Xu, and W. X. Shen, "Single-phase uninterruptible power supply based on Z-source inverter," *IEEE Trans. Ind. Electron.*, vol. 55, no. 8, pp. 2997–3004, Aug. 2008.
[94] W. Mo, P. C. Loh, and F. Blaabjerg, "Model predictive control for Z-source power converter," in *Proc. 8th Int. Conf. Power Electron. (ECCE Asia)*, May 2011, pp. 3022–3028.
[95] M. Mosa, O. Ellabban, A. Kouzou, H. Abu-Rub, and J. Rodriguez, "Model predictive control applied for quasi-Z-source inverter," in *Proc. 28th Annu. IEEE Appl. Power Electron. Conf. Expo. (APEC)*, Mar. 2013, pp. 165–169.
[96] J. Liu, S. Jiang, D. Cao, and F. Z. Peng, "A digital current control of quasi-Z-source inverter with battery," *IEEE Trans. Ind. Informat.*, vol. 9, no. 2, pp. 928–937, May 2013.
[97] J. Liu, S. Jiang, D. Cao, X. Lu, and F. Z. Peng, "Sliding-mode control of quasi-Z-source inverter with battery for renewable energy system," in *Proc. IEEE Energy Convers. Congr. Expo.*, Sep. 2011, pp. 3665–3671.
[98] J. W. Jung and A. Keyhani, "Control of a fuel cell based Z-source converter," *IEEE Trans. Energy Convers.*, vol. 22, no. 2, pp. 467–476, Jun. 2007.
[99] P. K. Pal, K. C. Jana, Y. P. Siwakoti, S. Majumdar, and F. Blaabjerg, "An active-neutral-point-clamped switched-capacitor multilevel inverter with quasi-resonant capacitor charging," *IEEE Trans. Power Electron.*, early access, Jul. 1, 2022, doi: 10.1109/TPEL.2022.3187736.
[100] H. K. Jahan, M. Sarhangzadeh, J. F. Ardashir, and F. Blaabjerg, "A symmetric switched-capacitor based basic inverter unit for grid-connected PV systems," *IEEE Trans. Power Electron.*, early access, Jun. 20, 2022, doi: 10.1109/TPEL.2022.3184757.
[101] A. Hota and V. Agarwal, "Novel switched capacitor quadruple boost inverter configuration for 3-ϕ induction motor drive," *IEEE J. Emerg. Sel. Topics Power Electron.*, early access, May 12, 2022, doi: 10.1109/JESTPE.2022.3174567.

IHAB JAMAL was born in Kafrelsheikh, Egypt, in 1978. He received the B.Sc. degree in electrical engineering from the Higher Technology Institute, 10th of Ramadan City, Egypt, in 2002. He is currently pursuing the M.Sc. degree. He worked as an Electrical Engineer at Tawam United Enterprise, in 2003, and was promoted until reached the Department Manager. His research interests include control, power electronics, and renewable energy.

MAHMOUD F. ELMORSHEDY (Member, IEEE) was born in Gharbeya, Egypt, in 1989. He received the B.Sc. and M.Sc. degrees in electrical engineering from Tanta University, Egypt, in 2012 and 2016, respectively, and the Ph.D. degree in electrical engineering from the School of Electrical and Electronic Engineering, Huazhong University of Science and Technology, China, in 2020. He worked as a Teaching Assistant with the Department of Electrical Power and Machines Engineering, Faculty of Engineering, Tanta University, in 2013, where he was promoted to an Assistant Lecturer, in June 2016. He is currently working as an Assistant Professor (On academic leave) with the Department of Electrical Power and Machines Engineering, Faculty of Engineering, Tanta University. He is also a Postdoctoral Fellow with the Renewable Energy Laboratory, College of Engineering, Prince Sultan University, Riyadh, Saudi Arabia. His research interests include linear induction motor, predictive control, power electronics, and renewable energy.

SHERIF M. DABOUR (Senior Member, IEEE) received the B.Sc. degree in electrical engineering from Zagazig University, Egypt, in 2002, and the M.Sc. and Ph.D. degrees in electrical power engineering from Tanta University, Egypt, in 2012 and 2015, respectively.

He has extensive experience in research and academic teaching in electrical power and industrial electronics. From 2003 to 2009, he worked as a Lecturer and a Certified Trainer at Technical and Vocational Training Corporation, Riyadh, Saudi Arabia. Since 2009, he has been joining Tanta University, where he is currently an Associate Professor (On academic leave). He was involved in many projects funded by the Egyptian Academy of Scientific Research and Technology and the Qatar National Research Foundation. He is also a Researcher-1A at Glasgow Caledonian University, U.K., where he is participating in research funded by the British Council and the Academy of Engineering and European Commission Projects. He has supervised ten M.Sc. students and three Ph.D. students. To date, he has published 49 articles in international journals and conferences in the field of his expertise. His research interests include analysis, modeling, and application of power electronics converters. In addition, he studies wind turbines, PV systems, storage systems, microgrids, electric vehicle chargers, and energy storage integration. He served as a Treasurer of the IEEE Power Electronics Society (PELS) Egypt Chapter, from 2017 to 2020. Additionally, he is a Reviewer of several journals, including IEEE TRANSACTIONS ON POWER ELECTRONICS AND INDUSTRIAL ELECTRONICS, *IET Power Applications*, and *IET Power Electronics*.

ESSAM M. RASHAD (Senior Member, IEEE) was born in Shebeen El-Kom, Egypt, in 1960. He received the B.Sc. degree from the Department of Electric Power and Machines Engineering, Faculty of Engineering, Menoufia University, Egypt, in 1983, and the M.Sc. and Ph.D. degrees from the Faculty of Engineering, Alexandria University, Egypt, in 1987 and 1992, respectively. From 1985 to 1990, he was an Offshore Electrical Engineer with Belayim Petroleum Company, Egypt. In 1992, he joined the Faculty of Engineering, Tanta University, Egypt, where he has been a Full Professor, since 2006. From February 2000 to August 2000, he was a Visiting Researcher with the Faculty of Engineering, Nagasaki University, Japan. In Summer 2003, he was a Visiting Researcher with the Faculty of Engineering and Applied Science, Memorial University of Newfoundland, St. John's, Canada. From 2004 to 2009, he was the Head of the Electrical Technology Department, Buraydah College of Technology, Saudi Arabia. From 2011 to 2014, he was the Vice Dean of Education and Student Affairs of the Faculty of Engineering, Tanta University. He was the Head of Electrical Power and Machines Engineering, from 2009 to 2011, and from 2014 to September 2020. He has published more than 160 technical conference and journal articles. His research interests include electrical machine analysis and design, electrical drives, power electronics, micro-grids, distributed generation, and renewable energy systems. He received the Outstanding Engineering Award for ''Outstanding Contribution in the Electrical Power Engineering Education, Research and Industry'' from IEEE-PES (Power and Energy Society), Egypt Chapter, in 2019. He was the General Chairperson of the 21st International Middle East Power Systems Conference (MEPCON'2019), Cairo, in December 2019, and the Co-Chairperson of the First IEEE Conference on Power Electronics and Renewable Energy, Aswan, Egypt, in October 2019.

WEI XU (Senior Member, IEEE) received the double B.E. and M.E. degrees from Tianjin University, Tianjin, China, in 2002 and 2005, respectively, and the Ph.D. degree from the Institute of Electrical Engineering, Chinese Academy of Sciences, in 2008, respectively, all in electrical engineering.

From 2008 to 2012, he made a Postdoctoral Fellow of the University of Technology Sydney, the Vice Chancellor Research Fellow with the Royal Melbourne Institute of Technology, and the Japan Science Promotion Society Invitation Fellow of Meiji University, respectively. Since 2013, he has been a Full Professor with the State Key Laboratory of Advanced Electromagnetic Engineering, Huazhong University of Science and Technology, China. His research interests include design and control of linear/rotary machines. He is a fellow of the Institute of Engineering and Technology (IET). He is the General Chair of 2021 International Symposium on Linear Drives for Industry Applications (LDIA 2021) and 2023 IEEE International Conference on Predictive Control of Electrical Drives and Power Electronics (PRECEDE 2023), in Wuhan, China. He has been an Editor or an Associate Editor for over ten internationally leading journals, such as IEEE TRANSACTIONS ON INDUSTRIAL ELECTRONICS, IEEE TRANSACTIONS ON VEHICULAR TECHNOLOGY, and IEEE TRANSACTIONS ON ENERGY CONVERSION.

DHAFER J. ALMAKHLES (Senior Member, IEEE) received the B.E. degree in electrical engineering from the King Fahd University of Petroleum and Minerals, Dhahran, Saudi Arabia, in 2006, and the master's (Hons.) and Ph.D. degrees from The University of Auckland, New Zealand, in 2011 and 2016, respectively. Since 2016, he has been with Prince Sultan University, Saudi Arabia, where he is currently the Chairperson of the Communications and Networks Engineering Department and the Director of the Science and Technology Unit. He is also the Leader of the Renewable Energy Research Team and the Renewable Energy Research Laboratory, Prince Sultan University. His research interests include the hardware implementation of control theory, signal processing, networked control systems, and sliding mode.